Neurobiology of Disease

Angiotensin-Converting Enzyme Converts Amyloid β-Protein 1–42 ($A\beta_{1-42}$) to $A\beta_{1-40}$, and Its Inhibition Enhances Brain Aβ Deposition

Kun Zou,[1,3] Haruyasu Yamaguchi,[4] Hiroyasu Akatsu,[5] Takaaki Sakamoto,[1] Mihee Ko,[1] Kazushige Mizoguchi,[2] Jian-Sheng Gong,[1] Wenxin Yu,[1] Takayuki Yamamoto,[5] Kenji Kosaka,[5] Katsuhiko Yanagisawa,[1] and Makoto Michikawa[1]

Departments of [1]Alzheimer's Disease Research and [2]Geriatric Medicine, National Institute for Longevity Sciences, National Center for Geriatrics and Gerontology, Obu, Aichi 474-8522, Japan, [3]Japan Society for the Promotion of Science, Tokyo 102-8471, Japan, [4]Gunma University School of Health Sciences, Maebashi 371-8514, Japan, and [5]Choju Medical Institute, Fukushimura Hospital, Toyohashi 441-8124, Japan

The abnormal deposition of the amyloid β-protein (Aβ) in the brain appears crucial to the pathogenesis of Alzheimer's disease (AD). Recent studies have suggested that highly amyloidogenic $A\beta_{1-42}$ is a cause of neuronal damage leading to AD pathogenesis and that monomeric $A\beta_{1-40}$ has less neurotoxicity than $A\beta_{1-42}$. We found that mouse and human brain homogenates exhibit an enzyme activity converting $A\beta_{1-42}$ to $A\beta_{1-40}$ and that the major part of this converting activity is mediated by the angiotensin-converting enzyme (ACE). Purified human ACE converts $A\beta_{1-42}$ to $A\beta_{1-40}$ as well as decreases $A\beta_{1-42}/A\beta_{1-40}$ ratio and degrades $A\beta_{1-42}$ and $A\beta_{1-40}$. Importantly, the treatment of Tg2576 mice with an ACE inhibitor, captopril, promotes predominant $A\beta_{1-42}$ deposition in the brain, suggesting that ACE regulates $A\beta_{1-42}/A\beta_{1-40}$ ratio *in vivo* by converting secreted $A\beta_{1-42}$ to $A\beta_{1-40}$ and degrading Aβs. The upregulation of ACE activity can be a novel therapeutic strategy for AD.

Key words: **angiotensin-converting enzyme; ACE; Alzheimer's disease; amyloid β-protein; Aβ; Aβ deposition; Aβ degradation; APP transgenic mouse**

Introduction

The progressive accumulation and deposition of the amyloid β-protein (Aβ) in the brain are early pathogenically important features of Alzheimer's disease (AD) (Selkoe, 2004). It has been assumed that insoluble Aβ amyloid is a culprit for inducing the pathological processes of AD, leading to neuronal dysfunction; however, recent studies have shown that not the insoluble form of Aβ but the soluble form of Aβ oligomers is pathogenic (Kirkitadze et al., 2002; Walsh et al., 2002). $A\beta_{1-42}$ is deposited early and selectively in senile plaques, and this deposition is an invariant feature of all forms of AD (Iwatsubo et al., 1994). A high $A\beta_{42}/A\beta_{40}$ ratio is a major determinant for AD development in familial AD with presenilin mutations (Borchelt et al., 1996; Duff et al., 1996; Scheuner et al., 1996; Citron et al., 1997).

Aβs ($A\beta_{1-40}$ and $A\beta_{1-42}$) are constantly secreted by many types of cell and are normally found in body fluids, including CSF. Recently, we have shown that monomeric $A\beta_{1-40}$ has neuroprotective effects against metal-induced oxidative damage and $A\beta_{1-42}$-induced neuronal death, whereas $A\beta_{1-42}$ is highly amyloidogenic and thus forms oligomers rapidly at very low concentrations, exerting strong neurotoxicity (Zou et al., 2002, 2003). $A\beta_{1-40}$, but not $A\beta_{1-42}$, rescues neurons from β- or γ-secretase inhibitor-induced cell death (Plant et al., 2003). Moreover, the inhibition of the effects of some nonsteroidal anti-inflammatory drugs, which reduce the risk of AD (in 't Veld et al., 2001), directly blocks $A\beta_{1-42}$ generation by changing presenilin conformation and shifting γ-secretase function toward the production of a shorter soluble Aβ (Weggen et al., 2001; Lleo et al., 2004).

A recent study demonstrated that $A\beta_{42}$ is essential for parenchymal and vascular amyloid deposition in mice and that mice expressing a high $A\beta_{1-40}$ level do not develop overt amyloid pathology (McGowan et al., 2005). Both $A\beta_{1-42}$ and $A\beta_{1-40}$ levels were elevated coordinately in late-onset sporadic AD brains (Selkoe, 2004) and non-AD human brains (Morishima-Kawashima et al., 2000); however, insoluble $A\beta_{42}$ level increases exponentially and steeply in an age-dependent manner, accompanied by much smaller increases in $A\beta_{40}$ level (Morishima-Kawashima et al., 2000). Thus, although it is still debatable whether $A\beta_{1-40}$ is nontoxic or neuroprotective, these findings suggest that decreasing neurotoxic $A\beta_{1-42}$ level could be a strategy for developing AD treatments.

We considered that there is a carboxyl peptidase that converts

Received Dec. 23, 2006; revised June 11, 2007; accepted June 29, 2007.

This work was supported by grants from the Ministry of Health, Labor, and Welfare of Japan (Research on Human Genome and Tissue Engineering Grant H17-004), the Program for Promotion of Fundamental Studies in Health of the National Institute of Biomedical Innovation, and Japan Society for the Promotion of Science, and Grant-in-Aid 18023046 for Scientific Research on Priority Areas-Research on Pathomechanisms of Brain Disorders from the Ministry of Education, Culture, Sports, Science, and Technology of Japan.

Correspondence should be addressed to Dr. Makoto Michikawa, Department of Alzheimer's Disease Research, National Institute for Longevity Sciences, National Center for Geriatrics and Gerontology, 36-3 Gengo, Morioka, Obu, Aichi 474-8522, Japan. E-mail: michi@nils.go.jp.

K. Zou's present address: Department of Neuroscience, Faculty of Pharmaceutical Sciences, Iwate Medical University, Yahaba 028-3694, Japan.

DOI:10.1523/JNEUROSCI.1549-07.2007

 0270-6474/07/278628-08$15.00/0

secreted neurotoxic $A\beta_{1-42}$ to $A\beta_{1-40}$, thus decreasing $A\beta_{42}/A\beta_{40}$ ratio. This notion has led us to experimentally identify an $A\beta_{1-42}$-to-$A\beta_{1-40}$-converting enzyme in the mouse and human brains. Interestingly, we found that the angiotensin-converting enzyme (ACE) is a major $A\beta_{1-42}$-to-$A\beta_{1-40}$-converting enzyme in the brain. This suggests that the modulation of ACE activity can be a novel therapeutic strategy for AD.

Materials and Methods

Captopril treatment of Tg2576 mice and tissue preparation. Male human amyloid precursor protein Swedish mutation (hAPPsw) transgenic Tg2576 mice were purchased from Taconic Farms (Germantown, NY). Mice at 6 months of age were fed with captopril-supplemented diet (0.25 mg/g) or control diet *ad libitum* for 7 or 11 months. There were 6–15 animals in each group. Animals were housed singly in individual cages. There were no significant differences in the amount of feed consumed or in the weight of the mice within or between treatment groups. The average captopril intake per animal was 30 mg/kg of body weight/d. Mice were killed by inhalation of CO_2, and 0.5 ml of blood was collected from the right atrium for the determination of serum ACE activity. Mice were then transcardially perfused with cold PBS. The left hemisphere of the brain was fixed in 4% buffered paraformaldehyde solution at 4°C for 48 h and incubated in 30% sucrose at 4°C for 48 h for histological processing. The right hemisphere of the brain was separated into the cerebral cortex, hippocampus, thalamus, and brainstem, and these samples were rapidly frozen in liquid nitrogen and stored at −80°C until analysis.

Human postmortem brain tissue. Frontal cortex tissue samples from autopsied control subjects ($n = 15$; male, 9, female, 6; neuropathological diagnosis, physiological aging) and AD subjects ($n = 15$; male, 9, female, 6; clinical and neuropathological diagnosis, AD) were obtained from Fukushimura Hospital (Toyohashi, Japan). Tissues were frozen immediately in liquid nitrogen at autopsy and then stored at −80°C until use. The average postmortem delay was 7.7 h and was not significantly different between the two groups. The average age of the subjects of the control group was 84.7 ± 1.9, and that of the subjects of the AD group was 85.5 ± 1.9 (data represent means ± SEM; $p = 0.75$, ANOVA, Bonferroni/Dunn test). Experiments using human brains were performed after obtaining the informed consent of the patients' guardians for diagnosis and biochemical, molecular biological, and genomic research. This study was examined and approved by the Ethics Committee of Fukushimura Hospital on October 6, 2005, and assigned the application number 180.

ACE activity assay. Cortical tissue (50–100 mg) was homogenized in a fourfold (w/v) volume of ACE homogenization buffer (50 mM HEPES, pH 7.4, 150 mM NaCl, 25 μM $ZnCl_2$, and 0.5% Triton X-100) and centrifuged at 4°C at 10,000 × *g* for 15 min. ACE activity in the supernatant against the synthetic substrate *N*-hippuryl-l-histidyl-l-leucine was determined using an ACE colorimetric kit (Buhlmann Laboratories, Schonenbuch, Switzerland). The reaction time was 6 h. ACE activity was then normalized by the initial weight of the brain tissue. For mouse serum ACE activity assay, serum was diluted at 1:2. All samples were measured in triplicate.

Western blot analysis for determining conversion of $A\beta_{1-42}$ to $A\beta_{1-40}$. Somatic ACE-deficient mice (002680) were obtained from The Jackson Laboratory (Bar Harbor, ME). $A\beta_{1-42}$ (Peptide Institute, Osaka, Japan) was freshly dissolved in 0.1% $NH_3.H_2O$ at 200 μM for each experiment. The wild-type mouse brain cortex, including the hippocampus, was homogenized in a twofold volume (w/v) of a buffer containing 10 mM Tris.HCl, pH 7.5, and 0.15 M NaCl, and the homogenate was centrifuged at 500 × *g* for 10 min. The supernatant was mixed with synthetic $A\beta_{1-42}$ to a final concentration of 30 μM and incubated at 37°C for 8 h. Ten microliters of the mixture was subjected to SDS-PAGE and blotted on a nitrocellulose membrane. To enhance the reactivity to an anti-$A\beta_{1-40}$ antibody, the membrane was boiled in PBS for 3 min after blotting, probed with an anti-$A\beta_{1-40}$ monoclonal antibody (1A10) (IBL, Takasaki, Japan), and visualized with SuperSignal (Pierce, Rockford, IL). Because of the high level of exogenous $A\beta_{1-42}$, the membrane was not boiled before the reaction with a polyclonal anti-$A\beta_{1-42}$ antibody.

Thioflavin-T binding assay for aggregated Aβ. Determination of the aggregated state of Aβ was performed on the basis of a previously established method (Levine, 1995, 1999). The incubated Aβ peptides were centrifuged at 17,000 × *g* for 60 min, the supernatant was removed, and the precipitate was suspended in 1 ml of 5 μM thioflavin-T in 50 mM glycine-NaOH, pH 8.5. Steady-state fluorescence intensities for each sample were determined as described previously (Zou et al., 2002).

Matrix-assisted laser desorption ionization-time of flight mass spectrometry. Purified human ACE (2 U/ml) (Millipore, Billerica, MA) was added to 30 μM $A\beta_{1-42}$ dissolved in 0.1% $NH_3.H_2O$ and incubated at 37°C for 6 h. Captopril (2 mM) was added to stop the digestion, and the sample was frozen in −80°C until use. The sample was subjected to matrix-assisted laser desorption/ionization-time of flight mass spectrometry (MALDI-TOF-MS) to detect the generation of $A\beta_{1-40}$. The same amount of ACE or $A\beta_{1-42}$ incubated alone under the same conditions as described above was used as control.

Biotinylation of $A\beta_{1-42}$ and determination of $A\beta_{1-42}$-to-$A\beta_{1-40}$-converting activity in human brain. $A\beta_{1-42}$ was biotinylated using a ProtOn biotin labeling kit (Vector Laboratories, Burlingame, CA). In brief, 0.5 mg of $A\beta_{1-42}$ was dissolved in DMSO and diluted with distilled water to 100 μl. $A\beta_{1-42}$ was biotinylated with a biotin-labeling reagent, and free biotin was removed using gel filtration slurry provided with the kit. The human frontal cortex tissue sample used was from a 76-year-old autopsied non-AD subject. The brain tissue was homogenized in a fourfold volume (w/v) of PBS, and the homogenate was mixed with biotinylated $A\beta_{1-42}$ at a concentration of 0.5 μg/μl. The mixtures were incubated at 37°C for 8 h with or without an ACE inhibitor (1 μM), namely captopril or enalapril. After incubation, 8 mM 3-[(3-cholamidopropyl)dimethylammonio]-1-propanesulfonate was added to extract Aβs. The samples were centrifuged at 4°C and 10,000 × *g* for 10 min, and the supernatant was applied to avidin agarose provided with the kit to purify biotinylated Aβs. Avidin agarose was washed with PBS four times, and biotinylated Aβs were eluted with 50 mM DTT in SDS-PAGE sample buffer. Biotinylated $A\beta_{1-40}$ converted from biotinylated $A\beta_{1-42}$ was detected by Western blot analysis using an anti-$A\beta_{1-40}$ monoclonal antibody (1A10).

Immunohistochemistry. The left hemispheres of the brains of Tg2576 mice were sagittally cut into 30 μm sections using a freezing microtome (RM 2145; Leica, Wetzlar, Germany). Thioflavin-S staining was performed as described previously (Wyss-Coray et al., 2001). For each mouse, thioflavin-S-positive plaques were counted in four to five sections per left hemisphere of the brain at a magnification of 40×. Serial sections were immunostained with anti-$A\beta_{1-40}$ and anti-$A\beta_{1-42}$ end-specific polyclonal antibodies, namely, RIB40 and RIB42, respectively (2 μg/ml; IBL), after a brief formic acid pretreatment, and immunopositive signals were visualized using an ABC elite kit (Vector Laboratories). Images of the cerebral cortex and hippocampus were captured using a digital camera attached to a microscope and analyzed using simple PCI software (Compix Imaging Systems, Lake Oswego, OR). $A\beta_{1-40}$ and $A\beta_{1-42}$ plaques were estimated as the percentage of immunostained area (positive pixels) divided by the examined area (total pixels). The quantification of thioflavin-S-positive plaques and areas attained by anti-$A\beta_{1-40}$ and anti-$A\beta_{1-42}$ antibodies was performed in a double-blind manner.

Aβ ELISA. Mouse cortices for ELISA were homogenized in 10 volumes of a mixture containing 5.0 M guanidine.HCl and 50 mM Tris.HCl, pH 8.0 (w/v), as described previously (Johnson-Wood et al., 1997). The brain homogenates were further diluted at 1:20 for 13-month-old and 1:500 for 17-month-old mice in a dilution buffer provided with the ELISA kit (Wako, Osaka, Japan). $A\beta_{1-42}$ and $A\beta_{1-40}$ standards (Peptide Institute) were prepared such that the final composition included the same concentration of guanidine. Purified human ACE (2 U/ml) with 10 μM $A\beta_{1-42}$ was diluted at 1:1000 with a dilution buffer containing complete protease inhibitor mixture (Roche, Mannheim, Germany). $A\beta_{1-42}$ and $A\beta_{1-40}$ levels were determined using the ELISA kit. Fibroblasts stably expressing human APP695 (Shiraishi et al., 2004) were grown in DMEM (Invitrogen, Grand Island, NY) containing 10% fetal calf serum. The medium was changed at 100% confluence, and the fibroblasts were treated with or without captopril. The levels of $A\beta_{1-40}$ and $A\beta_{1-42}$ in the medium were determined 24 h after the treatment of fibroblasts with captopril. All samples were measured in triplicate.

Results

We used two specific anti-$A\beta_{1-42}$ and anti-$A\beta_{1-40}$ antibodies to examine $A\beta_{1-40}$ generation in a tissue homogenate mixed with exogenously added synthetic $A\beta_{1-42}$. There was no cross-reaction between the two antibodies, which was confirmed by Western blot analysis (Fig. 1*A*). The coincubation of $A\beta_{1-42}$ with mouse cerebral homogenate generated $A\beta_{1-40}$, indicating the existence of an $A\beta_{1-42}$-to-$A\beta_{1-40}$-converting enzyme. Also, the generation of $A\beta_{1-40}$ from synthetic $A\beta_{1-42}$ was inhibited by the ACE inhibitors captopril and enalapril (Fig. 1*B*; supplemental Table 1, available at www.jneurosci.org as supplemental material). This converting activity was also found in the mouse cerebellum, kidney, heart, spleen, lung, skeletal muscle, and serum, indicating that the $A\beta_{1-42}$-to-$A\beta_{1-40}$-converting enzyme is distributed widely. In our Western blot system, neither endogenous $A\beta_{1-40}$ nor $A\beta_{1-42}$ was detected in these samples (data not shown). Moreover, Western blot analysis showed that the brain homogenate and serum from somatic ACE-deficient mice contain a markedly decreased capacity of generating $A\beta_{1-40}$ from $A\beta_{1-42}$ compared with those from wild-type (ACE+/+) and heterozygote (ACE+/−) mice (Fig. 1*C*). ACE is a dipeptidyl carboxypeptidase that catalyzes the cleavage of C-terminal dipeptides of several substrates and is widely distributed in mammalian tissues. These lines of evidence suggest that ACE in the brain homogenate plays a major role in the conversion of $A\beta_{1-42}$ to $A\beta_{1-40}$.

Thus, we next performed Western blot analysis, ELISA, and MALDI-TOF-MS to examine whether purified human ACE cleaves the 2 aa at the C terminus of synthetic $A\beta_{1-42}$ to generate $A\beta_{1-40}$. After the incubation of $A\beta_{1-42}$ with ACE, $A\beta_{1-40}$ level increased in a time-dependent manner, whereas $A\beta_{1-42}$ level decreased (Fig. 1*D*,*G*). Determination of the level of $A\beta_{1-40}$ generated and $A\beta_{1-42}$ remaining in the solution containing synthetic $A\beta_{1-42}$ and ACE shows that the levels of $A\beta_{1-40}$ and $A\beta_{1-42}$ were inversely and significantly correlated (supplemental Fig. 1*C*, available at www.jneurosci.org as supplemental material). $A\beta_{1-40}$ generation was completely inhibited by ACE inhibitors, namely, EDTA, captopril, and enalapril (Fig. 1*D*; supplemental Table 2, available at www.jneurosci.org as supplemental material). Because $A\beta_{1-42}$ can easily aggregate in aqueous buffers, it is important to understand whether ACE can mediate the cleavage of the aggregated form of $A\beta_{1-42}$. We performed thioflavin-T assay to monitor $A\beta_{1-42}$ aggregation. The thioflavin-T fluorescence of $A\beta_{1-42}$ incubated with or without ACE or of the mouse brain lysate showed no increase after 8 h of incubation. After 24 h of incubation, the thioflavin-T fluorescence of $A\beta_{1-42}$ incubated alone and with the brain homogenate markedly increased; however, ACE strongly inhibited the increase in thioflavin-T fluorescence (supplemental Fig. 1*A*, available at www.jneurosci.org as supplemental material). These results suggest that $A\beta_{1-40}$ is converted from nonfibril $A\beta_{1-42}$ within 8 h of incubation. We previously reported that $A\beta_{1-42}$ with random structures transformed to a β-sheet structure after 4 h of incubation at 37°C (Zou et al., 2003). Together with the present finding that the level of $A\beta_{1-40}$ converted from $A\beta_{1-42}$ increased until 8 h of incubation, it is possible that ACE generates $A\beta_{1-40}$ from $A\beta_{1-42}$ with both random and β-sheet structures.

Next we examined whether ACE degrades or converts aggregated $A\beta_{1-42}$. ACE did not reduce the thioflavin-T fluorescence of aggregated $A\beta_{1-42}$ after 24 h of incubation (supplemental Fig. 1*B*, available at www.jneurosci.org as supplemental material), and no $A\beta_{1-40}$ converted from $A\beta_{1-42}$ was detected by Western

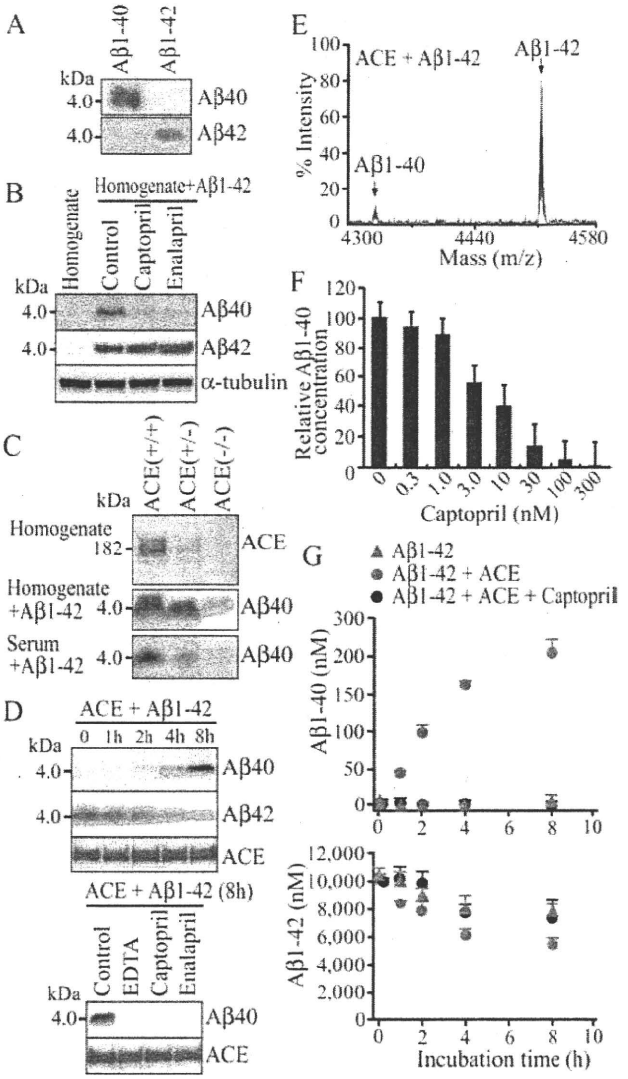

Figure 1. ACE converts $A\beta_{1-42}$ to $A\beta_{1-40}$. ***A***, We confirmed the specificities of monoclonal anti-$A\beta_{1-40}$ (1A10) and polyclonal anti-$A\beta_{1-42}$ antibodies. One microgram each of $A\beta_{1-40}$ and $A\beta_{1-42}$ was subjected to SDS-PAGE and then blotted onto a nitrocellulose membrane, and the membrane was probed with anti-$A\beta_{1-40}$ and anti-$A\beta_{1-42}$ antibodies. ***B***, Mouse brain homogenate was mixed with or without synthetic $A\beta_{1-42}$ and incubated at 37°C for 8 h. An anti-$A\beta_{1-40}$ antibody was used for detecting $A\beta_{1-40}$ generation. Captopril (1 μM) or enalapril (1 μM) markedly inhibited the generation of $A\beta_{1-40}$ from $A\beta_{1-42}$. ***C***, Top, The genotypes of ACE(+/+), ACE(+/−), and ACE(−/−) mice were confirmed by Western blot analysis of the brain homogenate using an anti-ACE polyclonal antibody (AF1513; R & D Systems). Middle, Bottom, Mouse brain homogenate (middle) or serum (bottom) was mixed with 30 μM $A\beta_{1-42}$ and incubated at 37°C for 8 h. The generation of $A\beta_{1-40}$ was detected by Western blot analysis. ***D***, Purified human ACE (2 U/ml) was mixed with synthetic $A\beta_{1-42}$ (30 μM), and the mixture was incubated at 37°C with or without ACE inhibitors. Top, $A\beta_{1-40}$ was generated in a time-dependent manner. Bottom, EDTA (10 μM), captopril (1 μM), and enalapril (1 μM) completely inhibited the conversion of $A\beta_{1-42}$ to $A\beta_{1-40}$. ***E***, MALDI-TOF-MS revealed a new peak with a mass of 4330 (corresponding to that of $A\beta_{1-40}$) after the incubation of $A\beta_{1-42}$ with ACE, indicating $A\beta_{1-40}$ generation. ***F***, Captopril blocked $A\beta_{1-40}$ generation in the mixture of $A\beta_{1-42}$ and purified human ACE in a dose-dependent manner. The density of $A\beta_{1-40}$ bands was measured by densitometry and normalized to the mean of the bands in the case of incubation without captopril. IC_{50} was estimated to be ~10 nM. ***G***, Time-dependent alterations in $A\beta_{1-42}$ and $A\beta_{1-40}$ levels in the solution of $A\beta_{1-42}$ (10 μM) alone; $A\beta_{1-42}$ (10 μM) and ACE (2 U/ml); or $A\beta_{1-42}$ (10 μM), ACE (2 U/ml), and captopril (1 μM). Each solution was incubated at 37°C for the time indicated. Ten microliters of each solution were collected at different time points and immediately frozen at −80°C until analysis. The levels of $A\beta_{1-42}$ and $A\beta_{1-40}$ in each sample were determined by ELISA. Data are the mean ± SEM of three samples.

Table 1. Kinetic parameters for conversion of Aβ1–42 to Aβ1–40 by human kidney ACE

Substrate	Product	K_m (μM)	k_{cat} (s^{-1})	k_{cat}/K_m (s^{-1}·mM^{-1})
$A\beta_{1-42}$	$A\beta_{1-40}$	7	4.2	600

$A\beta_{1-42}$ peptides (0, 2.5, 5, 10, 15, 20, 25, 30, and 50 μM) were incubated at 37°C for 8 h with human kidney ACE (0.45 μM). The level of $A\beta_{1-40}$ was determined by ELISA, and K_m, k_{cat}, and k_{cat}/K_m were then calculated.

blot analysis (data not shown), suggesting that ACE cannot degrade aggregated $A\beta_{1-42}$ or convert aggregated $A\beta_{1-42}$ to $A\beta_{1-40}$. MALDI-TOF-MS demonstrated peaks with molecular masses of 4330 and 4514 after incubation for 8 h, which matched the predicted masses of $A\beta_{1-40}$ and $A\beta_{1-42}$, respectively (Fig. 1*E*). MALDI-TOF-MS of the reaction mixture of ACE and $A\beta_{1-42}$ revealed several peaks with masses corresponding to those of $A\beta_{1-35}$, $A\beta_{1-34}$, $A\beta_{1-22}$, $A\beta_{1-20}$, and $A\beta_{1-19}$, in addition to $A\beta_{1-40}$. Interestingly, however, no $A\beta_{1-38}$, $A\beta_{1-7}$, or $A\beta_{8-42}$ was detected by our MALDI-TOF-MS. No $A\beta_{1-40}$ was detected by MALDI-TOF-MS in a solution of purified ACE or synthetic $A\beta_{1-42}$ after incubation at 37°C (supplemental Fig. 2, available at www.jneurosci.org as supplemental material). The IC_{50} of captopril needed for purified human ACE to convert $A\beta_{1-42}$ to $A\beta_{1-40}$ was ~10 nM, indicating the specific inhibitory effect of captopril on ACE-mediated $A\beta_{1-42}$-to-$A\beta_{1-40}$ conversion (Fig. 1*E*).

Next we determined the level of $A\beta_{1-40}$ converted from $A\beta_{1-42}$ and that of $A\beta_{1-42}$ remaining in the mixture of $A\beta_{1-42}$ and ACE using an ELISA kit. To determine the level of $A\beta_{1-42}$ lost from the solutions as a result of the "sticky" nature of $A\beta_{1-42}$, we also determined $A\beta_{1-42}$ level in the absence or presence of ACE with an ACE inhibitor as control. During the incubation of $A\beta_{1-42}$ with ACE for 2–8 h, ~10–20% of the degraded $A\beta_{1-42}$ was converted to $A\beta_{1-40}$. These results indicate that $A\beta_{1-40}$ can be generated from $A\beta_{1-42}$ through the action of ACE and that ACE cleaves $A\beta_{1-42}$ at other sites as well (Fig. 1*F*), which are supported by the results of MALDI-TOF-MS. Moreover, $A\beta_{40}/A\beta_{42}$ ratio increased during the incubation period, suggesting that ACE decreases $A\beta_{42}/A\beta_{40}$ ratio via its $A\beta_{1-42}$-to-$A\beta_{1-40}$-converting activity (data not shown). To understand the catalytic efficiency of ACE converting $A\beta_{1-42}$ to $A\beta_{1-40}$, we performed a kinetic assay of this conversion. The K_m, k_{cat}, and k_{cat}/K_m of the $A\beta_{1-42}$-to-$A\beta_{1-40}$ conversion by ACE were determined to be 7 μM, 4.2 s^{-1}, and 600 s^{-1}·mM^{-1}, respectively (Table 1). These values were similar to those of ACE for angiotensin I (Ang I) hydrolysis (Hayakari et al., 2003). Thus, this $A\beta_{1-42}$-to-$A\beta_{1-40}$ conversion activity of ACE is likely favorable *in vivo* under normal physiological conditions.

To determine whether the human brain shows this $A\beta_{1-42}$-to-$A\beta_{1-40}$-converting activity and whether the activity is inhibited by ACE inhibitors, we used the frontal cortex from a 76-year-old non-AD subject. To exclude the effect of endogenous $A\beta_{1-40}$, we labeled synthetic $A\beta_{1-42}$ with biotin. The sites of biotinylation were at lysine residues amino acid positions 16 and 28 in $A\beta_{1-42}$. The biotinylated Aβs were purified with avidin agarose, and biotinylated $A\beta_{1-40}$ generated from biotinylated $A\beta_{1-42}$ was detected by Western blot analysis. Similar to the results for the mouse brain homogenate, the incubation of $A\beta_{1-42}$ with the human brain homogenate resulted in the generation of $A\beta_{1-40}$, and this generation was inhibited by an ACE inhibitor, namely captopril or enalapril (Fig. 2*A*; supplemental Table 3, available at www.jneurosci.org as supplemental material). No endogenous $A\beta_{1-40}$ was detected in the human brain homogenate that was incubated without biotinylated $A\beta_{1-42}$ (Fig. 2*A*). These results indicate that the human brain also shows $A\beta_{1-42}$-to-$A\beta_{1-40}$-converting activity and that this activity is mainly mediated by ACE. To determine whether ACE activity and ACE expression level are altered in AD brains, we measured ACE activity and determined ACE expression level by Western blot analysis. AD brains showed reduced ACE activity and expression level compared with age-matched non-AD brains (Fig. 2*B–D*).

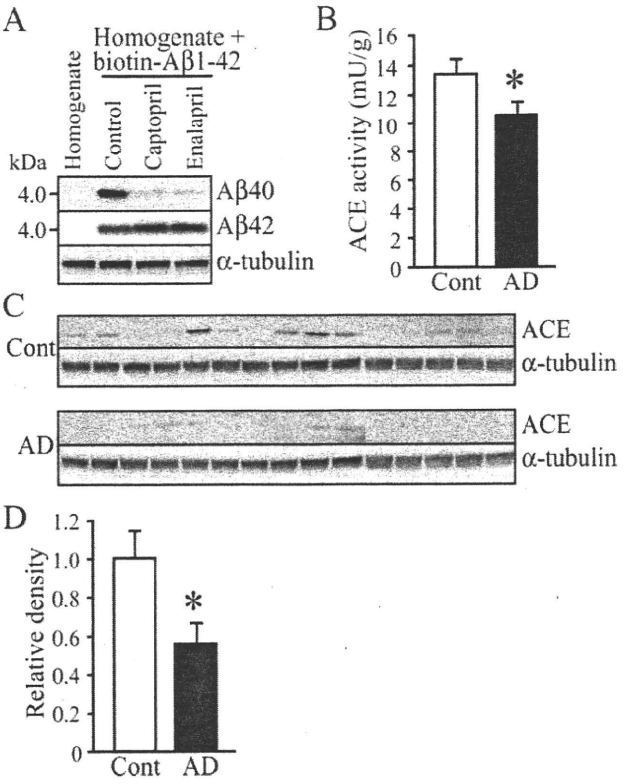

Figure 2. The human brain shows $A\beta_{1-42}$-to-$A\beta_{1-40}$-converting activity, and this ACE activity decreases in AD brain. ***A***, The frontal cortex from a non-AD subject was homogenized in PBS. Biotinylated $A\beta_{1-42}$ was added to the resulting homogenate, and the mixture was incubated at 37°C for 8 h with or without 1 μM ACE inhibitor, namely captopril or enalapril. Biotinylated Aβs were then purified using avidin agarose, and the conversion of $A\beta_{1-42}$ to $A\beta_{1-40}$ was detected by Western blot analysis using an anti-$A\beta_{1-40}$ monoclonal antibody (1A10) and an anti-$A\beta_{1-42}$ polyclonal antibody. ***B***, The cortices from the frontal gyri of the non-AD subjects and AD patients were homogenized in a lysis buffer. The resulting homogenate was centrifuged, and ACE activity in the supernatant was determined using an ACE colorimetric kit. The ACE activities of 15 non-AD control individuals (Cont) and 15 AD patients were measured. ***C***, The ACE expression level in the frontal cortex of those 30 subjects was determined by Western blot analysis, and a representative image is shown. Twenty micrograms of protein from the brain homogenate were subjected to SDS-PAGE and Western blot analysis. The membrane was probed with an anti-ACE polyclonal antibody. ***D***, The relative densities of the ACE bands were determined by densitometry. AD cases exhibited a significantly decreased ACE expression level. Data are the mean ± SEM of 15 samples. *$p < 0.05$ versus non-AD control by Mann–Whitney *U* test.

To determine whether ACE inhibition promotes AD pathology, we administered captopril, a blood–brain barrier-penetrating ACE inhibitor, to an AD mouse model (hAPPsw, Tg2576) (Hsiao et al., 1996) and assessed its effect on brain amyloid deposition. Tg2576 mice were fed with a captopril-supplemented diet (captopril, 30 mg/kg of body weight/d) from 6 months of age. The mice were killed at 13 and 17 months of age, and their brains were analyzed. In the 13-month-old mice, captopril treatment resulted in a trend toward an increase in the number of thioflavin-S-positive plaques ($n = 6$ per group; control neocortex, 27.9 ± 6.3; neocortex of captopril-treated mice, 34.9 ± 7.3; $p = 0.8728$; control hippocampus, 11.3 ± 3.2; hip-

pocampus of captopril-treated mice, 21.3 ± 5.8; $p = 0.2623$, Mann–Whitney U test). Interestingly, the ELISA of Aβs demonstrated a significantly higher $A\beta_{1-42}$ level in the neocortex of the 13-month-old captopril-treated mice than in that of the control mice (control, 504.6 ± 14.1 pmol/g; captopril-treated mice, 643.7 ± 49.0 pmol/g; $p = 0.0374$); however, the level of $A\beta_{1-40}$ remained unchanged (control, 1690.2 ± 141.4 pmol/g; captopril-treated mice, 1700.0 ± 249.8 pmol/g; $p = 0.9361$, Mann–Whitney U test). These results suggest that captopril treatment enhances $A\beta_{1-42}$ deposition to a greater extent than $A\beta_{1-40}$ deposition in the brain.

The analysis of the 17-month-old captopril-treated mice showed 2.5-fold and twofold increases in the number of thioflavin-S-positive plaques in the cortex and hippocampus, respectively, compared with that of the control mice (Fig. 3*B*,*G*). Moreover, $A\beta_{1-42}$-immunopositive areas in the neocortex and hippocampus were respectively 2.6-fold and twofold larger in the 17-month-old captopril-treated mice than in the control mice (Fig. 3*A*,*C*,*H*). Captopril treatment resulted in an increase in $A\beta_{1-40}$-immunopositive area; however, the increase was not statistically significant (Fig. 3*A*,*D*,*I*). These histological findings are supported by ELISA results. $A\beta_{1-42}$ level increased significantly higher (1.6-fold higher) in the neocortex of the captopril-treated mice than in that of the control mice, whereas $A\beta_{1-40}$ level showed no significant increase in the neocortex of the captopril-treated mice (Fig. 3*E*,*F*). Consistent with a previous study (Kawarabayashi et al., 2001), the present study also showed that small "diffuse plaques" appear to be labeled preferentially by the anti-$A\beta_{1-42}$ antibody, whereas big "cored plaques" are labeled by the anti-$A\beta_{1-40}$ antibody (Fig. 3*A*). Captopril treatment decreased serum ACE activity by 40% and neocortex ACE activity by 26% in the 17-month-old captopril-treated Tg2576 mice compared with that in the control mice (Fig. 3*J*,*K*). The activity of brain ACE significantly and inversely correlated with enhanced thioflavin-S-positive plaque formation in the neocortex of the mice (Fig. 3*L*). These findings indicate that ACE inhibition promotes a greater degree of and earlier $A\beta_{1-42}$ deposition than $A\beta_{1-40}$ deposition, suggesting that a low ACE activity in the brain promotes AD development by enhancing $A\beta_{1-42}$ deposition.

To determine whether acute ACE inhibition has a direct effect on the levels of brain Aβs, we treated Tg2576 mice with captopril by one-shot oral gavage. The Tg2576 mice used for this experiment were 9 months of age, younger than those used for chronic treatment and supposed to have few Aβ deposits. The one-shot oral gavage of captopril (30 mg/kg of body weight in a volume of 150 μl) to Tg2576 mice resulted in a significant decrease in serum ACE activity (control, 248 ± 21 U/L; captopril-treated mice, 43 ± 2 U/L; $p < 0.01$, Mann–Whitney U test; $n = 6$ each group). The ACE activity in the neocortex of the captopril-treated mice was significantly lower than that of the control mice (control, 38 ± 4 mU/L; captopril-treated, 32 ± 5 mU/L; Mann–Whitney U test, $p < 0.05$; $n = 6$ each group). However, the acute ACE inhibition resulted in no significant increase in the level of $A\beta_{1-42}$ (control, 391 ± 99 pmol/g; captopril-treated mice, 619 ± 94 pmol/g; $p = 0.15$, Mann–Whitney U test; $n = 6$ each group) or $A\beta_{1-40}$ (control, 929 ± 164 pmol/g; captopril-treated mice, 1270 ± 156 pmol/g; $p = 0.20$, Mann–Whitney U test; $n = 6$ each group) in the Tg2576 mouse brain. These results suggest that ACE inhibition does not significantly alter brain Aβ degradation in the acute phase.

To exclude the possibility that captopril affects γ-secretase processing, thereby altering $A\beta_{42}/A\beta_{40}$ ratio, we treated fibroblasts stably expressing hAPP695 with captopril and quantified the secreted $A\beta_{1-40}$ and $A\beta_{1-42}$. No cellular ACE in this cell line was detected by Western blot analysis using several anti-ACE antibodies [MAB3500 and MAB3502 (Millipore); ACENabm-9B9 (RDI, Flanders, NJ); 2E2 (Serotec, Oxford, UK); 19501 (QED Bioscience, San Diego, CA); AF1513 (R & D Systems, Minneapolis, MN)] (Fig. 4*A*) (data not shown). No ACE activity was detected in this cell line either (Fig. 4*B*). We used a mouse kidney homogenate as a positive control. ACE and ACE activity in the kidney homogenate were clearly detected, and ACE activity was inhibited by captopril (Fig. 4*A*,*B*). The treatment with captopril did not alter $A\beta_{1-40}$ or $A\beta_{1-42}$ level or $A\beta_{42}/A\beta_{40}$ ratio in fibroblasts, indicating that captopril has no effect on γ-secretase activity in terms of the shift from $A\beta_{1-42}$ secretion to $A\beta_{1-40}$ secretion (Figs. 4*C*,*D*). These results suggest that the enhanced predominant $A\beta_{1-42}$ deposition in the captopril-treated Tg2576 mice is caused by the inhibition of ACE-mediated $A\beta_{1-42}$-to-$A\beta_{1-40}$-converting activity and $A\beta_{1-42}$ and $A\beta_{1-40}$ degradations, and not by altering γ-secretase processing.

Discussion

Here, we reported for the first time that ACE converts $A\beta_{1-42}$ to $A\beta_{1-40}$ and that a chronic inhibition of ACE enhances predominant $A\beta_{1-42}$ deposition *in vivo*. A high $A\beta_{1-42}$ level or a high $A\beta_{42}/A\beta_{40}$ ratio appears crucial in AD pathogenesis. Although their molecular mechanisms are not yet fully understood, $A\beta_{1-40}$ and $A\beta_{1-42}$ generations are supposed to be modulated by the shift of γ-cleavage (Weggen et al., 2001; De Strooper, 2003; Lleo et al., 2004). In addition to the γ-cleavage shift theory, $A\beta_{1-40}$ and $A\beta_{1-42}$ have recently been suggested to be generated from a longer form of Aβ species generated by ε-cleavage at every three residues in its carboxyl portion; however, the enzyme involved in carboxypeptidyl cleavage has not yet been identified (Qi-Takahara et al., 2005). Our present study showed a novel catabolism pathway for modulating $A\beta_{1-42}$ degradation; that is, ACE generates $A\beta_{1-40}$ from secreted $A\beta_{1-42}$ by carboxydipeptidyl cleavage in the mouse and human brains.

ACE is a zinc metallopeptidase and a dipeptidyl carboxypeptidase that cleaves 2 aa from the C terminus of Ang I and converts Ang I to the vasoactive and aldosterone-stimulating peptide Ang II (Corvol et al., 1995). ACE is a membrane-bound enzyme in endothelial cells and several types of epithelial and neuroepithelial cells. The active site of ACE is located in the extracellular space, and the unbound form of ACE circulating in biological fluids, such as plasma and CSF, and both types of ACE have enzymatic activity (Zubenko et al., 1985; Rigat et al., 1990; Sibony et al., 1993). These lines of evidence support our findings that ACE converts $A\beta_{1-42}$ to $A\beta_{1-40}$ and degrades Aβs under physiological conditions, thereby contributing to the prevention of Aβ deposition in the brain. In this study, ~10–20% of degraded $A\beta_{1-42}$ was converted to $A\beta_{1-40}$ in the presence of ACE.

Previous studies showed that the major cleavage site of $A\beta_{1-40}$ is between amino acid positions 7 and 8 (Hu et al., 2001; Oba et al., 2005). If the $A\beta_{1-40}$ generated from $A\beta_{1-42}$ was subsequently cleaved between amino positions 7 and 8 by ACE, then $A\beta_{8-40}$ could have been detected by MALDI-TOF-MS. However, no generation of $A\beta_{1-7}$, $A\beta_{8-40}$, or $A\beta_{8-42}$ in the reaction mixture of ACE and $A\beta_{1-42}$ was detected by MALDI-TOF-MS, indicating that no cleavage between amino positions 7 and 8 occurs in our system. What causes this discrepancy remains undetermined. It is possible that $A\beta_{1-42}$ and $A\beta_{1-40}$ have different conformations, which may allow ACE to access these species differently. Another explanation may be that the ACE used in this study contained the plasma membrane domain from the human kidney, and that

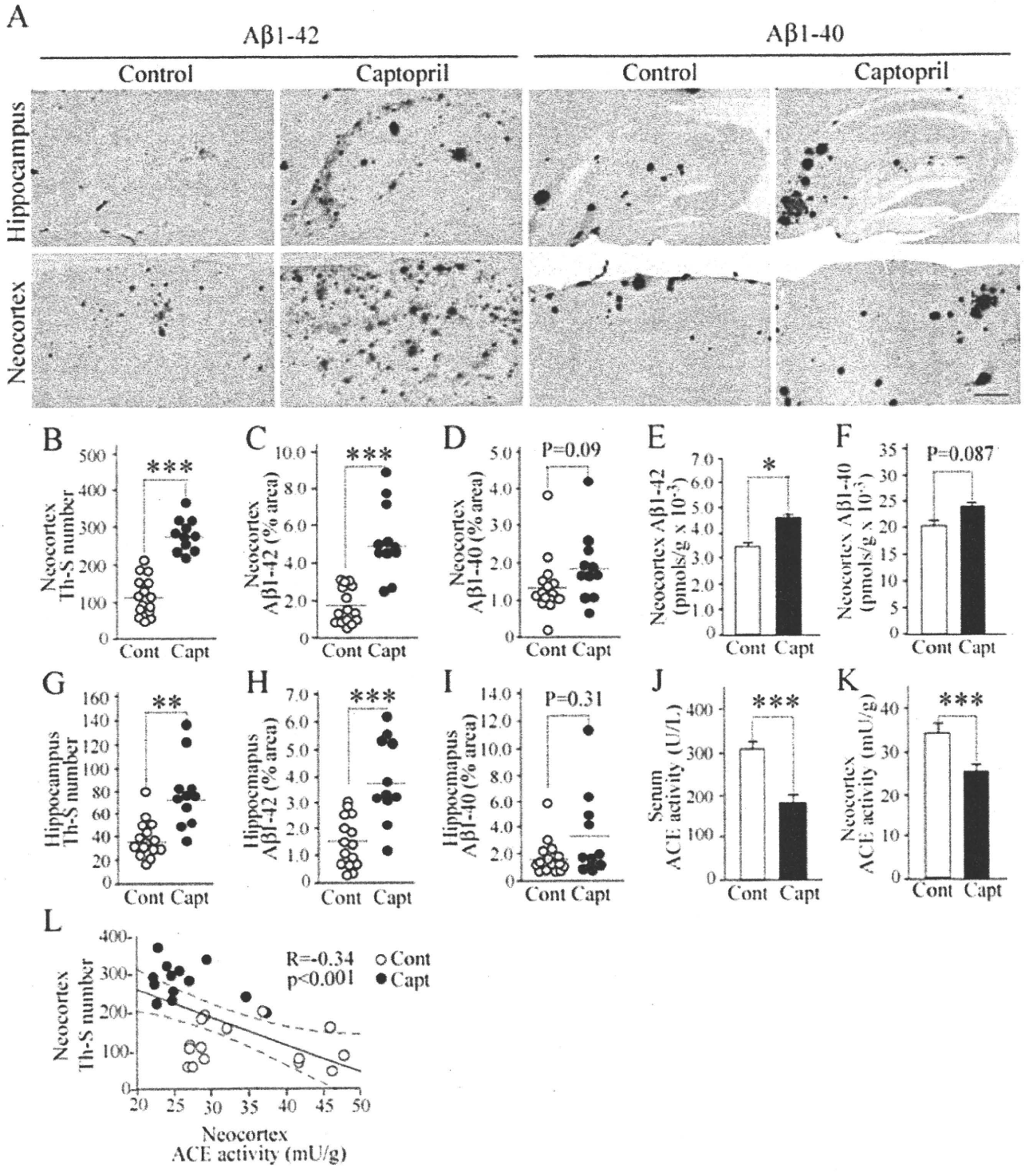

Figure 3. Long-term inhibition of ACE activity enhances $A\beta_{1-42}$ deposition in the 17-month-old hAPPsw transgenic mouse (Tg2576) brain. Tg2576 mice at 6 months of age were treated with captopril (30 mg/kg of body weight/d) and killed after 11 months of treatment. ***A***, Sagittal brain sections of 17-month-old control diet-fed and captopril-supplemented diet-fed mice were stained with antibodies specific for $A\beta_{1-42}$ and $A\beta_{1-40}$ to detect human $A\beta$ deposition. Representative images of hippocampi and neocortices with or without treatment are shown. The left four panels are images immunostained by the anti-$A\beta_{1-42}$ antibody, and the right four panels are images of brain sections immunostained by the anti-$A\beta_{1-40}$ antibody. Scale bar, 500 μm. ***B–I***, Determinations of the number of thioflavin-S-positive plaques (***B***, ***G***) and immunopositive area demonstrated by anti-$A\beta_{1-42}$ antibody (***C***, ***H***) and anti-$A\beta_{1-40}$ antibody (***D***, ***I***) in brain neocortex (***B–D***) and hippocampus [***G–I***; $n = 15$ for control diet (Cont; open circles); $n = 11$ for captopril diet (Capt; filled circles)]. ***E***, ***F***, $A\beta_{1-42}$ (***E***) and $A\beta_{1-40}$ (***F***) levels determined by ELISA in brain neocortex of 17-month-old mice fed with control and captopril-supplemented diets. The ELISA data included both soluble and insoluble $A\beta$s. ***J***, ***K***, Serum (***J***) and neocortex (***K***) ACE activities in mice fed with control diet and captopril-supplemented diet. ***L***, Significant inverse correlation between ACE activity and the number of thioflavin-S-positive plaques in neocortex. Data are the mean ± SEM; p was determined by the Mann–Whitney U test (***B–K***) and Spearman rank test (***L***). $^*p < 0.05$; $^{**}p < 0.01$; $^{***}p < 0.001$.

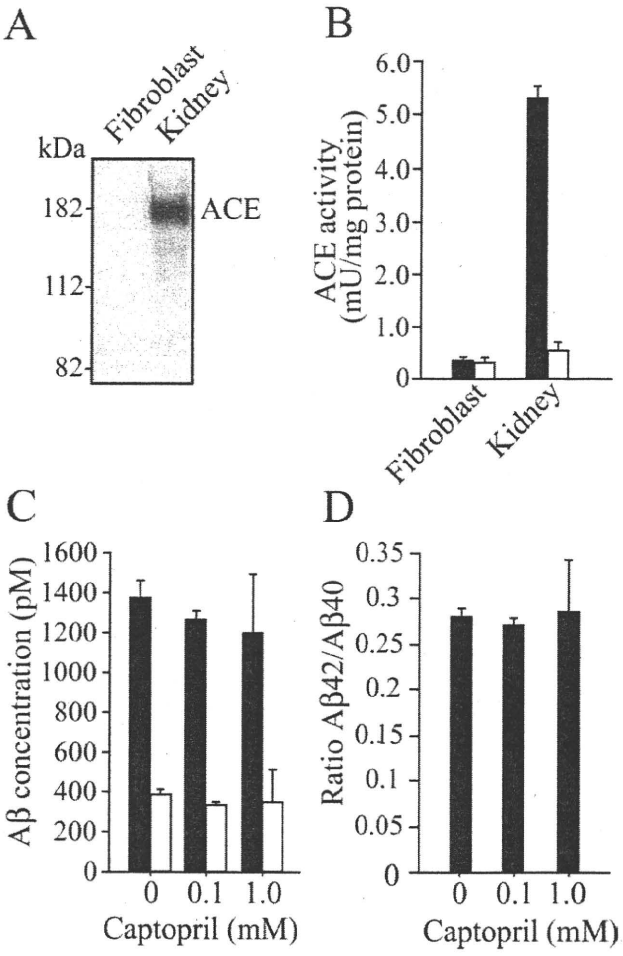

Figure 4. Effect of captopril on $A\beta_{1-42}/A\beta_{1-40}$ ratio in hAPP-expressing fibroblasts. ***A***, Fibroblast homogenate and wild-type mouse kidney homogenate (40 μg of protein) were subjected to Western blot analysis using an anti-ACE polyclonal antibody. No cellular ACE in fibroblasts was detected, whereas ACE in the mouse kidney homogenate as a positive control was clearly detected. ***B***, ACE activities in the fibroblast and kidney homogenates were determined. ACE activity in the fibroblast homogenate was very low, whereas that in kidney homogenate was detectable, which was clearly inhibited by captopril (1 μM) treatment (filled bars, no captopril; open bars, captopril). ***C***, Fibroblasts stably expressing human APP695 were grown in DMEM containing 10% FBS. The cells were treated with or without captopril at 100% confluence after changing the culture medium. The $A\beta_{1-40}$ and $A\beta_{1-42}$ levels in the medium were determined by ELISA after 24 h. Filled bars, $A\beta_{1-40}$; open bars, $A\beta_{1-42}$. ***D***, $A\beta_{42}/A\beta_{40}$ ratio was calculated. ***C***, ***D***, Note that captopril did not alter the levels of secreted Aβs (***C***) or $A\beta_{42}/A\beta_{40}$ ratio (***D***).

used in previous studies was the secreted form of ACE in human seminal plasma or Cos7-secreted conditioned media. Additional studies are required to clarify this. In this study, MALDI-TOF-MS demonstrated a peak corresponding to $A\beta_{1-40}$ in the reaction mixture of ACE and $A\beta_{1-42}$ but no peak corresponding to Aβ1–38. This suggests that ACE does not cleave the 2 C-terminal amino acids of $A\beta_{1-40}$.

In addition, one may question why $A\beta_{1-40}$ level increases if $A\beta_{1-40}$ can be digested further. It is possible that the most predominant substrate at the start of the reaction is $A\beta_{1-42}$ and that the degradation of $A\beta_{1-40}$ is negligible because the level of $A\beta_{1-40}$ generated from $A\beta_{1-42}$ is extremely low (Fig. 1*F*).

To understand the role of ACE *in vivo*, we induced a chronic ACE inhibition in Tg2576 mice and found that the ACE inhibition enhances Aβ deposition *in vivo*. However, it is important to determine whether acute and short-term treatment with captopril also increases brain soluble Aβ level. To exclude the effect of Aβ deposition, we used younger Tg2576 mice, whose brain shows almost no Aβ deposition (Kawarabayashi et al., 2001), in this experiment. An acute, one-shot oral administration of captopril to the young Tg2576 mice resulted in a significant decrease in serum and brain ACE activities; however, the level of brain $A\beta_{1-42}$ or $A\beta_{1-40}$ was not significantly affected. A recent *in vivo* study also shows that ACE inhibitors at doses similar to those used clinically do not increase the levels of brain Aβs (Eckman et al., 2006). Previous studies using purified human seminal plasma ACE and cultured cells showed that ACE degrades Aβs and ACE inhibition increases Aβ levels in APP- and ACE-transfected cells (Hu et al., 2001; Hemming and Selkoe, 2005; Oba et al., 2005). However, these findings seem to disagree with those of *in vivo* studies. One explanation may be that other Aβ-degrading enzymes, such as neprilysin, the insulin-degrading enzyme, and the endothelin-converting enzyme may compensate for the acute reduction in ACE activity *in vivo*. An important issue to be stressed is that even a high captopril dose induces only a slight decrease in brain ACE activity; however, long-term captopril treatment induces a marked and significant enhancement of Aβ deposition in the aged mouse brain. Thus, additional studies are required to determine the chronic effect of ACE inhibitors at clinical doses on AD pathology and development.

Numerous studies have shown that the I allele of ACE *D/I* polymorphism is associated with an increased risk of late-onset AD (Hu et al., 1999; Kehoe et al., 1999; Elkins et al., 2004; Lehmann et al., 2005) and that *I* polymorphism is associated with a decreased serum ACE level (Rigat et al., 1990). ACE activity in CSF from patients with a moderately severe senile dementia of the AD type has been shown to decrease to 41% of that in CSF from non-AD patients (Zubenko et al., 1985). Because ACE inhibitors are widely used in patients with hypertension, which is a risk factor for AD, it is important to determine the effects of ACE inhibitors on Aβ deposition *in vivo*. We have treated an AD mouse model (hAPPsw, Tg2576) (Hsiao et al., 1996) with captopril, a blood–brain barrier-penetrating ACE inhibitor, and found that, consistent with our *in vitro* findings, treatment with captopril enhances the depositions of $A\beta_{1-42}$ and $A\beta_{1-40}$, but more prominently that of $A\beta_{1-42}$ in mouse brains. This suggests that a certain amount of $A\beta_{1-40}$ is generated by ACE from secreted $A\beta_{1-42}$ and that treatment with ACE inhibitors may be a risk factor for AD. There have been very few clinical studies analyzing the effects of ACE inhibitors on AD development and cognitive decline in AD patients, and results to date are inconclusive (Birkenhager et al., 2004; Gard and Rusted, 2004; Ohrui et al., 2004; Khachaturian et al., 2006). Therefore, additional studies are required to determine the effects of ACE inhibitors both on Aβ deposition in the brain of patients during long-term medication with ACE inhibitors and on the cognitive ability of AD patients without hypertension. Together, the results of this study suggest that the upregulation of ACE activity may decrease $A\beta_{42}/A\beta_{40}$ ratio and the levels of Aβs and can be used as a strategy for developing novel therapeutic regimens for AD patients without hypertension.

References

Birkenhager WH, Forette F, Staessen JA (2004) Dementia and antihypertensive treatment. Curr Opin Nephrol Hypertens 13:225–230.

Borchelt DR, Thinakaran G, Eckman CB, Lee MK, Davenport F, Ratovitsky T, Prada CM, Kim G, Seekins S, Yager D, Slunt HH, Wang R, Seeger M, Levey AI, Gandy SE, Copeland NG, Jenkins NA, Price DL, Younkin SG, Sisodia SS (1996) Familial Alzheimer's disease-linked presenilin 1 variants elevate Aβ1–42/1–40 ratio in vitro and in vivo. Neuron 17:1005–1013.

Citron M, Westaway D, Xia W, Carlson G, Diehl T, Levesque G, Johnson-Wood K, Lee M, Seubert P, Davis A, Kholodenko D, Motter R, Sherrington R, Perry B, Yao H, Strome R, Lieberburg I, Rommens J, Kim S, Schenk D, et al. (1997) Mutant presenilins of Alzheimer's disease increase production of 42-residue amyloid β-protein in both transfected cells and transgenic mice. Nat Med 3:67–72.

Corvol P, Williams TA, Soubrier F (1995) Peptidyl dipeptidase A: angiotensin I-converting enzyme. Methods Enzymol 248:283–305.

De Strooper B (2003) Aph-1, Pen-2, and Nicastrin with presenilin generate an active γ-secretase complex. Neuron 38:9–12.

Duff K, Eckman C, Zehr C, Yu X, Prada CM, Perez-tur J, Hutton M, Buee L, Harigaya Y, Yager D, Morgan D, Gordon MN, Holcomb L, Refolo L, Zenk B, Hardy J, Younkin S (1996) Increased amyloid-β42(43) in brains of mice expressing mutant presenilin 1. Nature 383:710–713.

Eckman EA, Adams SK, Troendle FJ, Stodola BA, Kahn MA, Fauq AH, Xiao HD, Bernstein KE, Eckman CB (2006) Regulation of steady-state β-amyloid levels in the brain by neprilysin and endothelin-converting enzyme but not angiotensin-converting enzyme. J Biol Chem 281:30471–30478.

Elkins JS, Douglas VC, Johnston SC (2004) Alzheimer disease risk and genetic variation in ACE: a meta-analysis. Neurology 62:363–368.

Gard PR, Rusted JM (2004) Angiotensin and Alzheimer's disease: therapeutic prospects. Expert Rev Neurother 4:87–96.

Hayakari M, Satoh K, Izumi H, Kudoh T, Asano J, Yamazaki T, Tsuchida S (2003) Kinetic-controlled hydrolysis of Leu-Val-Val-hemorphin-7 catalyzed by angiotensin-converting enzyme from rat brain. Peptides 24:1075–1082.

Hemming ML, Selkoe DJ (2005) Amyloid β-protein is degraded by cellular angiotensin-converting enzyme (ACE) and elevated by an ACE inhibitor. J Biol Chem 280:37644–37650.

Hsiao K, Chapman P, Nilsen S, Eckman C, Harigaya Y, Younkin S, Yang F, Cole G (1996) Correlative memory deficits, Aβ elevation, and amyloid plaques in transgenic mice. Science 274:99–102.

Hu J, Miyatake F, Aizu Y, Nakagawa H, Nakamura S, Tamaoka A, Takahash R, Urakami K, Shoji M (1999) Angiotensin-converting enzyme genotype is associated with Alzheimer disease in the Japanese population. Neurosci Lett 277:65–67.

Hu J, Igarashi A, Kamata M, Nakagawa H (2001) Angiotensin-converting enzyme degrades Alzheimer amyloid β-peptide (Aβ); retards Aβ aggregation, deposition, fibril formation; and inhibits cytotoxicity. J Biol Chem 276:47863–47868.

in 't Veld BA, Ruitenberg A, Hofman A, Launer LJ, van Duijn CM, Stijnen T, Breteler MM, Stricker BH (2001) Nonsteroidal antiinflammatory drugs and the risk of Alzheimer's disease. N Engl J Med 345:1515–1521.

Iwatsubo T, Odaka A, Suzuki N, Mizusawa H, Nukina N, Ihara Y (1994) Visualization of Aβ42(43) and Aβ40 in senile plaques with end-specific Aβ monoclonals: evidence that an initially deposited species is Aβ42(43). Neuron 13:45–53.

Johnson-Wood K, Lee M, Motter R, Hu K, Gordon G, Barbour R, Khan K, Gordon M, Tan H, Games D, Lieberburg I, Schenk D, Seubert P, McConlogue L (1997) Amyloid precursor protein processing and Aβ42 deposition in a transgenic mouse model of Alzheimer disease. Proc Natl Acad Sci USA 94:1550–1555.

Kawarabayashi T, Younkin LH, Saido TC, Shoji M, Ashe KH, Younkin SG (2001) Age-dependent changes in brain, CSF, and plasma amyloid β-protein in the Tg2576 transgenic mouse model of Alzheimer's disease. J Neurosci 21:372–381.

Kehoe PG, Russ C, McIlory S, Williams H, Holmans P, Holmes C, Liolitsa D, Vahidassr D, Powell J, McGleenon B, Liddell M, Plomin R, Dynan K, Williams N, Neal J, Cairns NJ, Wilcock G, Passmore P, Lovestone S, Williams J, et al. (1999) Variation in DCP1, encoding ACE, is associated with susceptibility to Alzheimer disease. Nat Genet 21:71–72.

Khachaturian AS, Zandi PP, Lyketsos CG, Hayden KM, Skoog I, Norton MC, Tschanz JT, Mayer LS, Welsh-Bohmer KA, Breitner JC (2006) Antihypertensive medication use and incident Alzheimer disease: the Cache County Study. Arch Neurol 63:686–692.

Kirkitadze MD, Bitan G, Teplow DB (2002) Paradigm shifts in Alzheimer's disease and other neurodegenerative disorders: the emerging role of oligomeric assemblies. J Neurosci Res 69:567–577.

Lehmann DJ, Cortina-Borja M, Warden DR, Smith AD, Sleegers K, Prince JA, van Duijn CM, Kehoe PG (2005) Large meta-analysis establishes the ACE insertion-deletion polymorphism as a marker of Alzheimer's disease. Am J Epidemiol 162:305–317.

Levine III H (1995) Soluble multimeric Alzheimer β(1–40) pre-amyloid complexes in dilute solution. Neurobiol Aging 16:755–764.

Levine III H (1999) Quantification of β-sheet amyloid fibril structures with thioflavin T. Methods Enzymol 309:274–284.

Lleo A, Berezovska O, Herl L, Raju S, Deng A, Bacskai BJ, Frosch MP, Irizarry M, Hyman BT (2004) Nonsteroidal anti-inflammatory drugs lower Aβ42 and change presenilin 1 conformation. Nat Med 10:1065–1066.

McGowan E, Pickford F, Kim J, Onstead L, Eriksen J, Yu C, Skipper L, Murphy MP, Beard J, Das P, Jansen K, Delucia M, Lin WL, Dolios G, Wang R, Eckman CB, Dickson DW, Hutton M, Hardy J, Golde T (2005) Aβ42 is essential for parenchymal and vascular amyloid deposition in mice. Neuron 47:191–199.

Morishima-Kawashima M, Oshima N, Ogata H, Yamaguchi H, Yoshimura M, Sugihara S, Ihara Y (2000) Effect of apolipoprotein E allele epsilon4 on the initial phase of amyloid β-protein accumulation in the human brain. Am J Pathol 157:2093–2099.

Oba R, Igarashi A, Kamata M, Nagata K, Takano S, Nakagawa H (2005) The N-terminal active centre of human angiotensin-converting enzyme degrades Alzheimer amyloid β-peptide. Eur J Neurosci 21:733–740.

Ohrui T, Tomita N, Sato-Nakagawa T, Matsui T, Maruyama M, Niwa K, Arai H, Sasaki H (2004) Effects of brain-penetrating ACE inhibitors on Alzheimer disease progression. Neurology 63:1324–1325.

Plant LD, Boyle JP, Smith IF, Peers C, Pearson HA (2003) The production of amyloid β-peptide is a critical requirement for the viability of central neurons. J Neurosci 23:5531–5535.

Qi-Takahara Y, Morishima-Kawashima M, Tanimura Y, Dolios G, Hirotani N, Horikoshi Y, Kametani F, Maeda M, Saido TC, Wang R, Ihara Y (2005) Longer forms of amyloid β-protein: implications for the mechanism of intramembrane cleavage by γ-secretase. J Neurosci 25:436–445.

Rigat B, Hubert C, Alhenc-Gelas F, Cambien F, Corvol P, Soubrier F (1990) An insertion/deletion polymorphism in the angiotensin I-converting enzyme gene accounting for half the variance of serum enzyme levels. J Clin Invest 86:1343–1346.

Scheuner D, Eckman C, Jensen M, Song X, Citron M, Suzuki N, Bird TD, Hardy J, Hutton M, Kukull W, Larson E, Levy-Lahad E, Viitanen M, Peskind E, Poorkaj P, Schellenberg G, Tanzi R, Wasco W, Lannfelt L, Selkoe D, et al. (1996) Secreted amyloid β-protein similar to that in the senile plaques of Alzheimer's disease is increased in vivo by the presenilin 1 and 2 and APP mutations linked to familial Alzheimer's disease. Nat Med 2:864–870.

Selkoe DJ (2004) Cell biology of protein misfolding: the examples of Alzheimer's and Parkinson's diseases. Nat Cell Biol 6:1054–1061.

Shiraishi H, Sai X, Wang HQ, Maeda Y, Kurono Y, Nishimura M, Yanagisawa K, Komano H (2004) PEN-2 enhances γ-cleavage after presenilin heterodimer formation. J Neurochem 90:1402–1413.

Sibony M, Gasc JM, Soubrier F, Alhenc-Gelas F, Corvol P (1993) Gene expression and tissue localization of the two isoforms of angiotensin I converting enzyme. Hypertension 21:827–835.

Walsh DM, Klyubin I, Fadeeva JV, Cullen WK, Anwyl R, Wolfe MS, Rowan MJ, Selkoe DJ (2002) Naturally secreted oligomers of amyloid β-protein potently inhibit hippocampal long-term potentiation in vivo. Nature 416:535–539.

Weggen S, Eriksen JL, Das P, Sagi SA, Wang R, Pietrzik CU, Findlay KA, Smith TE, Murphy MP, Bulter T, Kang DE, Marquez-Sterling N, Golde TE, Koo EH (2001) A subset of NSAIDs lower amyloidogenic Aβ42 independently of cyclooxygenase activity. Nature 414:212–216.

Wyss-Coray T, Lin C, Yan F, Yu GQ, Rohde M, McConlogue L, Masliah E, Mucke L (2001) TGF-beta1 promotes microglial amyloid-β clearance and reduces plaque burden in transgenic mice. Nat Med 7:612–618.

Zou K, Gong JS, Yanagisawa K, Michikawa M (2002) A novel function of monomeric amyloid β-protein serving as an antioxidant molecule against metal-induced oxidative damage. J Neurosci 22:4833–4841.

Zou K, Kim D, Kakio A, Byun K, Gong JS, Kim J, Kim M, Sawamura N, Nishimoto S, Matsuzaki K, Lee B, Yanagisawa K, Michikawa M (2003) Amyloid β-protein (Aβ)1–40 protects neurons from damage induced by Aβ1–42 in culture and in rat brain. J Neurochem 87:609–619.

Zubenko GS, Volicer L, Direnfeld LK, Freeman M, Langlais PJ, Nixon RA (1985) Cerebrospinal fluid levels of angiotensin-converting enzyme in Alzheimer's disease, Parkinson's disease and progressive supranuclear palsy. Brain Res 328:215–221.

DOI:10.1158/1078-0432.CCR-07-4144

Imaging, Diagnosis, Prognosis

Inverse Correlation between Tumoral Indoleamine 2,3-Dioxygenase Expression and Tumor-Infiltrating Lymphocytes in Endometrial Cancer: Its Association with Disease Progression and Survival

Kazuhiko Ino,[1] Eiko Yamamoto,[1] Kiyosumi Shibata,[1] Hiroaki Kajiyama,[1] Norio Yoshida,[1] Mikio Terauchi,[1] Akihiro Nawa,[1] Tetsuro Nagasaka,[2] Osamu Takikawa,[3] and Fumitaka Kikkawa[1]

Abstract

Purpose: Tumor escape from host immune systems is a crucial mechanism for disease progression. We recently showed that the immunosuppressive enzyme indoleamine 2,3-dioxygenase (IDO) is a prognostic indicator for endometrial cancer. The purpose of the present study was to investigate the relationship between IDO expression and tumor-infiltrating lymphocytes (TIL) or natural killer (NK) cells and to clarify their prognostic effect in endometrial cancer.

Experimental Design: Immunohistochemical staining for IDO expression in endometrial cancer tissues (n = 65) was done. Tumor-infiltrating CD3+ and CD8+ lymphocytes, as well as CD57+ NK cells, were counted in serial tissue sections.

Results: High IDO expression in tumor cells was found in 32 of 65 cases and was positively correlated with myometrial invasion, nodal metastasis, and lymph-vascular space involvement. We also found a significant correlation between high IDO expression and reduced numbers of CD3+, CD8+, and CD57+ cells infiltrating into both the tumor epithelium and stroma. Patients with high IDO expression, a low number of stromal CD3 (<60), low intraepithelial CD8 (<25), or low stromal CD8 (<40) had significantly impaired progression-free survival. On multivariate analysis, IDO expression and the number of stromal CD3+ TILs were independent prognostic factors for impaired progression-free survival.

Conclusions: Tumoral IDO expression correlated with a reduced number of TILs and NK cells in endometrial cancer, possibly contributing to disease progression and impaired clinical outcome. These findings suggest that targeting IDO to restore host antitumor immunity may be a therapeutic strategy for endometrial cancer.

Tumor escape from host immune surveillance creates a state of "tolerance" and is a crucial mechanism for cancer progression (1). However, its underlying cellular and molecular basis remains poorly understood. Recent studies suggest that one mechanism that may contribute to this tolerance is the immunoregulatory enzyme indoleamine 2,3-dioxygenase (IDO; ref. 2).

IDO is an intracellular enzyme that catalyzes the initial and rate-limiting steps in the metabolism of the essential amino acid tryptophan along the kynurenine pathway (3). Recently, evidence that indicates an immunosuppressive function for IDO has been accumulating. It was first found that IDO is expressed in the mouse placenta during pregnancy and prevents rejection of the allogeneic fetus, thereby suggesting involvement of IDO in fetal-maternal tolerance (4). Subsequent studies clarified the mechanism of IDO immunosuppression to be local depletion of tryptophan and/or production of toxic tryptophan catabolites, causing growth arrest and the apoptosis of alloreactive T cells or natural killer (NK) cells that are extremely sensitive to tryptophan shortage (5). The tryptophan-derived catabolite kynurenine also inhibits the expression of specific triggering receptors on NK cells and regulates NK-cell function (6).

In malignancy, it was firstly shown that IDO is expressed by the tumor cells themselves in various human cancers and that tumors expressing IDO can resist immune rejection by tumor-associated antigen-specific host cytotoxic T cells in mouse models (7). Furthermore, IDO is also expressed by certain subsets of dendritic cells in tumor-draining lymph nodes in mice, and these IDO-expressing dendritic cells potently suppress host antitumor T-cell responses and induce tolerance to tumor-derived antigens (8, 9). More recently, it was shown that IDO inhibitors potentiated the antitumor activity of chemotherapeutic agents in tumor-bearing mice, suggesting the involvement of IDO in chemoresistance (10, 11). Evidence from these animal studies has prompted further examination of the clinical relevance of IDO in human cancers.

Authors' Affiliations: [1]Department of Obstetrics and Gynecology and [2]Division of Pathology/Clinical Laboratory, Nagoya University Graduate School of Medicine, Nagoya, Japan and [3]National Institute for Longevity Sciences, National Center for Geriatrics and Gerontology, Obu, Japan

Received 9/10/07; revised 11/30/07; accepted 12/3/07.

Grant support: Japanese Ministry of Education, Culture, Sports, Science, and Technology grant-in-aid 18591831 (K. Ino).

The costs of publication of this article were defrayed in part by the payment of page charges. This article must therefore be hereby marked *advertisement* in accordance with 18 U.S.C. Section 1734 solely to indicate this fact.

Requests for reprints: Kazuhiko Ino, Department of Obstetrics and Gynecology, Nagoya University Graduate School of Medicine, 65 Tsurumai-cho, Showa-ku, Nagoya 466-8550, Japan. Phone: 81-52-744-2261; Fax: 81-52-744-2268; E-mail: kazuino@med.nagoya-u.ac.jp.

doi:10.1158/1078-0432.CCR-07-4144

DOI:10.1158/1078-0432.CCR-07-4144

Several limited studies showed that expression of IDO is associated with poor clinical outcome in malignant melanoma (9), ovarian cancer (12), lung cancer (13), and colorectal cancer (14). We have recently shown that high IDO expression in endometrial cancer tissues is positively correlated with disease progression and impaired patient survival, suggesting that IDO is a prognostic indicator for endometrial cancer (15). However, the functional significance of IDO in human cancers remains to be clarified.

In the current study, we investigated the relationship between IDO expression and the degree of tumor infiltration of T cells or NK cells in endometrial cancer using immunohistochemical staining. We also attempted to elucidate whether the number of tumor-infiltrating lymphocytes (TIL) and level of IDO expression are related to disease progression and survival in endometrial cancer patients.

Materials and Methods

Patients and case selection. Sixty-five patients with endometrial endometrioid adenocarcinoma who underwent surgical treatment at Nagoya University Hospital between 1992 and 2001 were included in this study. Surgical treatment consisted of total abdominal hysterectomy and bilateral salpingo-oophorectomy and followed by surgical staging, including peritoneal washing cytology and lymphadenectomy. Patients with histologic cell types other than endometrioid adenocarcinoma, such as papillary serous or clear cell, were not included in this study. The mean age of the patients was 57.7 y. All patients were staged according to the 1988 International Federation of Gynecology and Obstetrics (FIGO) criteria: 44 were stage I (4 were IA, 27 were IB, 13 were IC), 6 were stage II, 9 were stage III, and 6 were stage IV. Histologic grade was assigned according to the criteria of WHO classification: 31 were G_1, 23 were G_2, and 11 were G3. In this study, all patients with FIGO stage IC and higher received postoperative chemotherapy with six cycles of either cisplatin/doxorubicin/cyclophosphamide or cisplatin/etoposide in 1992 to 1999 and paclitaxel/carboplatin after 2000. Patients receiving postoperative radiation therapy or any preoperative treatment were excluded from this study because their number was very small. Patients with tumor recurrence were treated with chemotherapy, local radiation therapy, or surgical resection, if possible.

Antibodies. Antihuman IDO monoclonal antibody was prepared as described previously (16). The reactivity and specificity of this monoclonal antibody was confirmed via Western blot analysis of tumor tissue samples, where IDO protein was detected as a 42-kDa single band (15). A rabbit polyclonal antibody against human CD3, a marker of T cells, was purchased from Dako, and a mouse monoclonal antibody against human CD8, a marker of cytotoxic T cells, was purchased from Nichirei. In addition, a mouse monoclonal antibody against human CD57 was purchased from Bécton Dickinson. The CD57 antigen is one of the markers for a subset of NK cells and has been used for immunohistochemical evaluation of tumor-infiltrating NK cells in many previous reports (17–20).

Immunohistochemistry. Informed consent was obtained from individual patients for the use of their tissue samples. Surgical specimens were fixed in 10% formalin and embedded in paraffin. Paraffin specimens were cut at a thickness of 4 μm. For heat-induced epitope retrieval, deparaffinized sections were soaked in Target Retrieval Solution (Dako) and incubated at 95°C for 15 min in a microwave oven. Immunohistochemical staining was done using the avidin-biotin immunoperoxidase technique. Endogenous peroxidase activity was blocked by incubation with 0.3% H_2O_2 in methanol for 15 min, and nonspecific immunoglobulin binding was blocked by incubation with 10% normal goat serum for 10 min. Sections were incubated at room temperature for 2 h with primary antibodies against IDO, CD3, CD8, and CD57. The sections were rinsed and incubated for 30 min with the biotinylated second antibody. After washing, the sections were incubated for 30 min with horseradish peroxidase–conjugated streptavidin and finally treated with 3,3′-diaminobenzidine tetrahydrochloride in 0.01% H_2O_2 for 10 min. The slides were counterstained with Meyer's hematoxylin. As a negative control, the primary antibody was replaced with normal mouse or rabbit IgG at an appropriate dilution. As a positive control for IDO immunostaining, tissue sections of normal placenta were used as previously reported (21).

Scoring of IDO expression in tumor cells. IDO expression levels were classified semiquantitatively based on the percentage of tumor cells with IDO staining and the staining intensity. The percentage positivity was scored as 0 if <5% of cells were stained (negative), 1 if 5% to 30% (sporadic), 2 if 30% to 70% (focal), and 3 if >70% (diffuse), whereas the staining intensity was scored as 0 if there was no staining, 1 if cells were weakly stained, and 2 if strongly stained (equal to the positive control level). The final IDO expression score was defined as follows: IDO- if the sum of the percentage positivity score and the staining intensity score was 0 to 1, IDO1+ if the sum was 2 to 3, and IDO2+ if the sum was 4 to 5. In this scoring system, IDO expression in the tumor stromal cells was not considered because IDO immunostaining in nontumor cells was not remarkable or absent in all cases examined. In each case, three different areas were evaluated, and the mean of the results was considered to be the final IDO expression score. The scoring procedure was carried out by two independent observers (each blinded to the other's score) without any knowledge of the clinical data. The concordance rate was over 95% between the observers.

Quantification of TILs and NK cells within tumors. Tumor-infiltrating CD3+ and CD8+ T cells were classified into two groups by their localization: (*a*) intraepithelial, cells infiltrating into the tumor epithelium, and (*b*) stromal, cells infiltrating the tumor stroma adjacent to cancer epithelia or the stroma along the invasive margin of the cancer epithelia. Three independent areas with the most abundant lymphocyte infiltration were selected, and the intraepithelial TILs and stromal TILs were independently counted in each microscopic field at 200× (0.0625 mm^2). The average count for three areas was accepted as the number of TILs in each case. CD57+ NK cells were similarly counted at 200× in the three areas with the most abundant infiltration. Because the number of tumor-infiltrating CD57+ cells was very low, the total count of both intraepithelial and stromal cells was taken.

Statistical analysis. Pearson χ^2 test was used to analyze the correlation of IDO expression with clinicopathologic variables or the number of TILs. Comparison of the numbers of TILs between IDO-/IDO1+ and IDO2+ groups was done using the Mann-Whitney *U* test. Overall survival and progression-free survival (PFS) were calculated from the date of surgery to the date of death and the date of progression/recurrence, respectively, or date of last follow-up. Survival analyses were done according to the Kaplan-Meier method. Comparison of survival between groups was done with the log-rank test. Cox proportional hazard model and stepwise analysis were used for univariate and multivariate analyses. SAS software (SAS Institute, Inc.) was used for all statistical analyses, and a P value of <0.05 was considered significant.

Results

Immunohistochemical expression of IDO in endometrial cancer tissues. As shown in Fig. 1A-D, IDO immunoreactivity was detected at variable levels and was localized to the cytoplasm of tumor cells. In contrast, IDO immunoreactivity in the tumor stroma was very faint or absent. Based on the IDO expression score in tumor cells, all cases were classified into two groups: high IDO expression (IDO2+) and no or low IDO expression (IDO- or IDO1+). Of the 65 specimens examined, high IDO

DOI:10.1158/1078-0432.CCR-07-4144

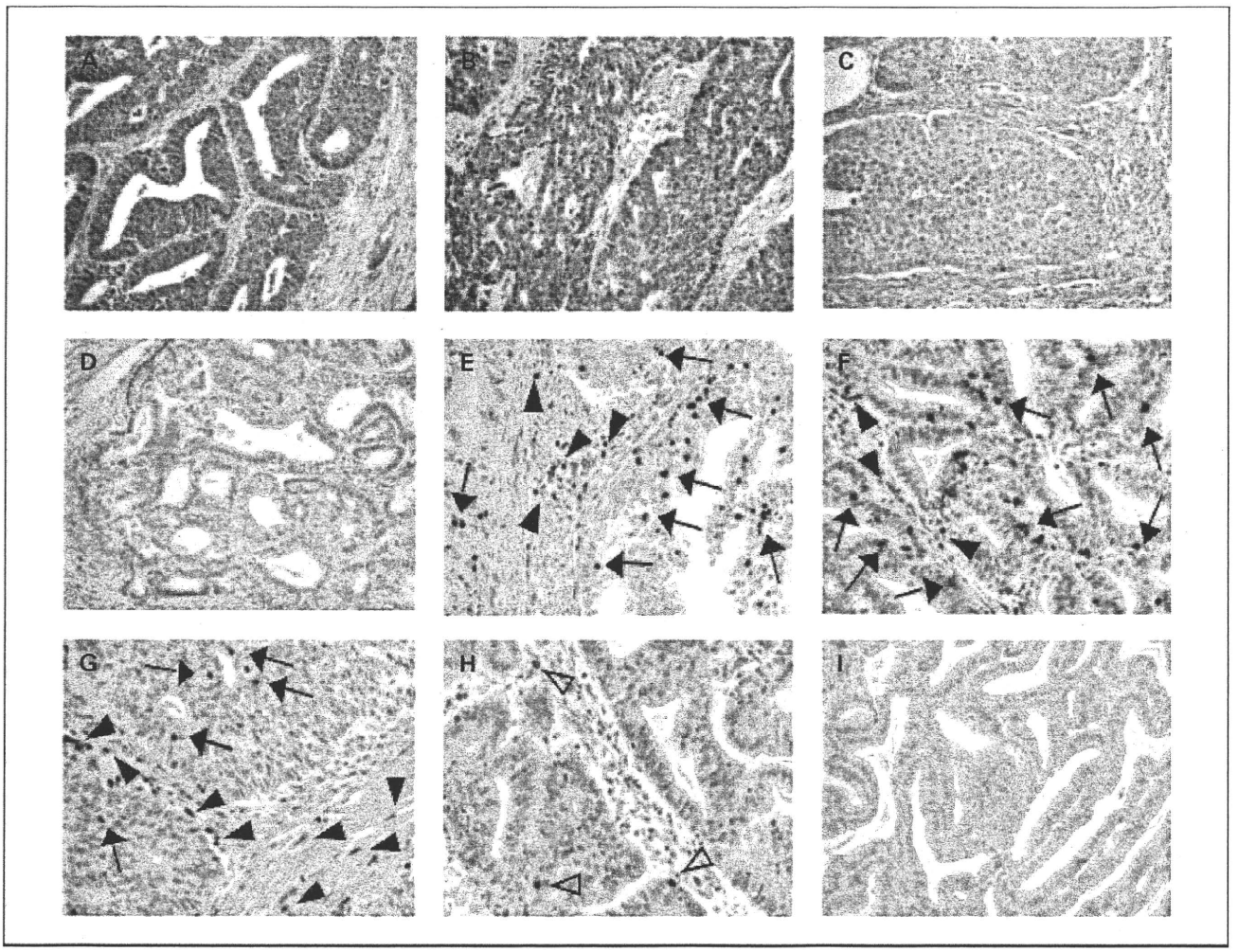

Fig. 1. *A-D,* representative immunohistochemical staining for IDO in endometrial cancer tissues. Marked IDO expression in grade 1 (*A*), grade 2 (*B*), and grade 3 (*C*) adenocarcinomas, and no IDO expression in grade 1 adenocarcinoma (*D*). *E-H,* representative immunohistochemical staining for TILs and NK cells. *E,* CD3+ cells; *F* and *G,* CD8+ cells; *H,* CD57+ cells. Arrows, intraepithelial TILs; arrowheads, stromal TILs; open arrowheads, tumor-infiltrating NK cells. I, negative control. Original magnification, 100× (*A-D* and *I*) and 200× (*E-H*).

expression was found in 32 cases (49%), whereas IDO- and IDO1+ tumors were found in 13 (20%) and 20 (31%) cases, respectively.

The correlations of high IDO expression with clinicopathologic variables is summarized in Table 1. High IDO expression was positively correlated with FIGO stage ($P = 0.001$), depth of myometrial invasion ($P = 0.004$), lymph node metastasis ($P = 0.035$), and lymph-vascular space involvement ($P = 0.001$), but not with histologic grade ($P = 0.741$). These results suggest that high IDO expression is strongly associated with disease progression in endometrial cancer.

Association of IDO expression with the infiltration of TILs. Next, we evaluated the number of T cells and NK cells infiltrating into the tumor epithelium or tumor stroma (Fig. 1E-H) to investigate the relationship between IDO expression and TILs. The number of intraepithelial CD3+ cells in IDO2+ tumors (range, 3-55; median, 28) was significantly lower ($P = 0.0094$) than in IDO-/IDO1+ tumors (range, 7-78; median, 41; Fig. 2A), whereas the number of stromal CD3+ cells in IDO2+ tumors (range, 14-95; median, 48) was significantly lower ($P < 0.0001$) than in IDO-/IDO1+ tumors (range, 30-142; median, 75; Fig. 2B). Similarly, the number of intraepithelial CD8+ cells in IDO2+ tumors (range, 1-48; median, 18) was significantly lower ($P = 0.0013$) than in IDO-/IDO1+ tumors (range, 3-58; median, 29; Fig. 2C) and the number of stromal CD8+ cells in IDO2+ tumors (range, 8-68; median, 24) was also significantly lower ($P < 0.0001$) than in IDO-/IDO1+ tumors (range, 14-118; median, 55; Fig. 2D). Furthermore, the number of CD57+ cells in IDO2+ tumors (range, 0-16; median, 2) was significantly lower ($P = 0.0139$) than in IDO-/IDO1+ tumors (range, 0-20; median, 4; Fig. 2E).

The correlation of IDO expression and TIL counts is summarized in Table 1. High IDO expression was significantly correlated with low numbers of intraepithelial CD3+ cells ($P = 0.018$), stromal CD3+ cells ($P = 0.001$), intraepithelial CD8+ cells ($P = 0.001$), stromal CD8+ cells ($P = 0.001$), and total CD57+ cells ($P = 0.025$).

Correlation of IDO expression and TIL counts with patient survival. The median follow-up period was 72 months (range, 5-148). During the follow-up period, disease progression/recurrence was observed in 14 cases (21.5%) in which

DOI:10.1158/1078-0432.CCR-07-4144

nine patients (13.8%) died of the disease. The overall survival rates of patients with IDO-/IDO1+ tumors and IDO2+ tumors were 95.7% and 73.1%, respectively, whereas the PFS rates for IDO-/IDO1+ and IDO2+ were 97.0% and 56.5%, respectively (Fig. 3A). Patients with high IDO expression (IDO2+) had significantly impaired PFS (P = 0.0001) when compared with patients with weak or no expression of IDO (IDO-/IDO1+; Fig. 3A).

Next, we analyzed the effect of the TIL count on patient survival. As shown in Fig. 3B and C, the PFS rates for high (≥35) and low (<35) intraepithelial CD3 groups were 87.1% and 68.8%, respectively, whereas the PFS rates for high (≥60) and low (<60) stromal CD3 groups were 93.9% and 59.4%, respectively. Patients with low (<60) stromal CD3+ cell counts had significantly impaired PFS (P = 0.0011) when compared with patients with high (≥60) stromal CD3+ cell counts (Fig. 3C). Similarly, the PFS rates for high (≥25) and low (<25) intraepithelial CD8 groups were 89.3% and 68.7%, respectively, whereas the PFS rates for high (≥40) and low (<40) stromal CD8 groups were 96.6% and 61.4%, respectively (Fig. 3D and E). There was a significant difference in the PFS between high and low intraepithelial CD8 groups (P = 0.0493) and between high and low stromal CD8 groups (P = 0.0011; Fig. 3D and E). In contrast, the PFS rates for high (≥5) and low (<5) CD57 groups were 86.7% and 72.8%, respectively, with no significant difference in the PFS between the two groups (P = 0.1689; Fig. 3F).

Multivariate analysis of prognostic variables in endometrial cancer patients. Univariate analysis showed that FIGO stage (P = 0.002), nodal status (P = 0.001), lymph-vascular space involvement (P = 0.020), IDO expression (P = 0.024), and stromal CD8 count (P = 0.041) were significant prognostic factors for overall survival (Table 2). Among these variables, only FIGO stage [hazard ratio (HR) = 2.456, P = 0.032] and nodal status (HR = 4.904, P = 0.026) were independent prognostic factors with respect to overall survival on multivariate analysis. In contrast, FIGO stage (P = 0.001), nodal status (P = 0.010), lymph-vascular space involvement (P = 0.031), IDO expression (P = 0.005), stromal CD3 count (P = 0.006), intraepithelial CD8 count (P = 0.044), and stromal CD8 count (P = 0.012) were significant prognostic factors for PFS on univariate analysis. Among these variables, FIGO stage (HR = 3.878, P = 0.019), IDO expression (HR = 6.317, P = 0.025), and stromal CD3 count (HR = 3.693, P = 0.047) were

Table 1. Correlation of IDO expression with clinicopathologic factors and the number of TILs

Characteristics	Patients, *n* (%)	High IDO expression, *n* (%)	*P*
All cases	65 (100)	32 (49.2)	
Clinicopathologic factors			
Age (y)			
<60	41 (63.1)	21 (51.2)	
≥60	24 (36.9)	11 (45.8)	0.675
FIGO stage			
I/II	50 (76.9)	19 (38.0)	
III/IV	15 (23.1)	13 (86.7)	0.001
Grade			
G1-G2	54 (83.1)	26 (48.1)	
G3	11 (16.9)	6 (54.5)	0.741
Myometrial invasion			
≤50%	39 (60.0)	13 (33.3)	
>50%	26 (40.0)	19 (73.1)	0.004
Nodal status			
Negative	59 (90.8)	26 (44.1)	
Positive	6 (9.2)	6 (100.0)	0.035
LVSI			
Absent	40 (61.5)	13 (32.5)	
Present	25 (38.5)	19 (76.0)	0.001
No. TILs*			
Intraepithelial CD3+			
High (≥35)	32 (49.2)	11 (34.4)	
Low (<35)	33 (50.8)	21 (63.6)	0.018
Stromal CD3+			
High (≥60)	33 (50.8)	8 (24.2)	
Low (<60)	32 (49.2)	24 (75.0)	0.001
Intraepithelial CD8+			
High (≥25)	29 (44.6)	8 (27.6)	
Low (<25)	36 (55.4)	24 (66.7)	0.001
Stromal CD8+			
High (≥40)	29 (44.6)	4 (13.8)	
Low (<40)	36 (55.4)	28 (77.8)	0.001
Total CD57+			
High (<5)	23 (35.4)	7 (30.4)	
Low (<5)	42 (64.6)	25 (59.5)	0.025

Abbreviation: LVSI, lymph-vascular space involvement.
*TILs were counted with a microscopic field at 200× (0.0625 mm^2).

DOI:10.1158/1078-0432.CCR-07-4144

significantly independent prognostic factors with respect to PFS on multivariate analysis.

Discussion

Recent reports showed that the immunoregulatory enzyme IDO is associated with poor clinical outcome in various human cancers (12–14). We also reported that high IDO expression is associated with the impaired patient survival in endometrial cancer (15), although its functional mechanism has not yet been identified. Thus, in the present study, to clarify the relationship between IDO expression and the local immunologic status in endometrial cancer, we immunohistochemically analyzed the tumoral IDO expression, as well as the numbers of

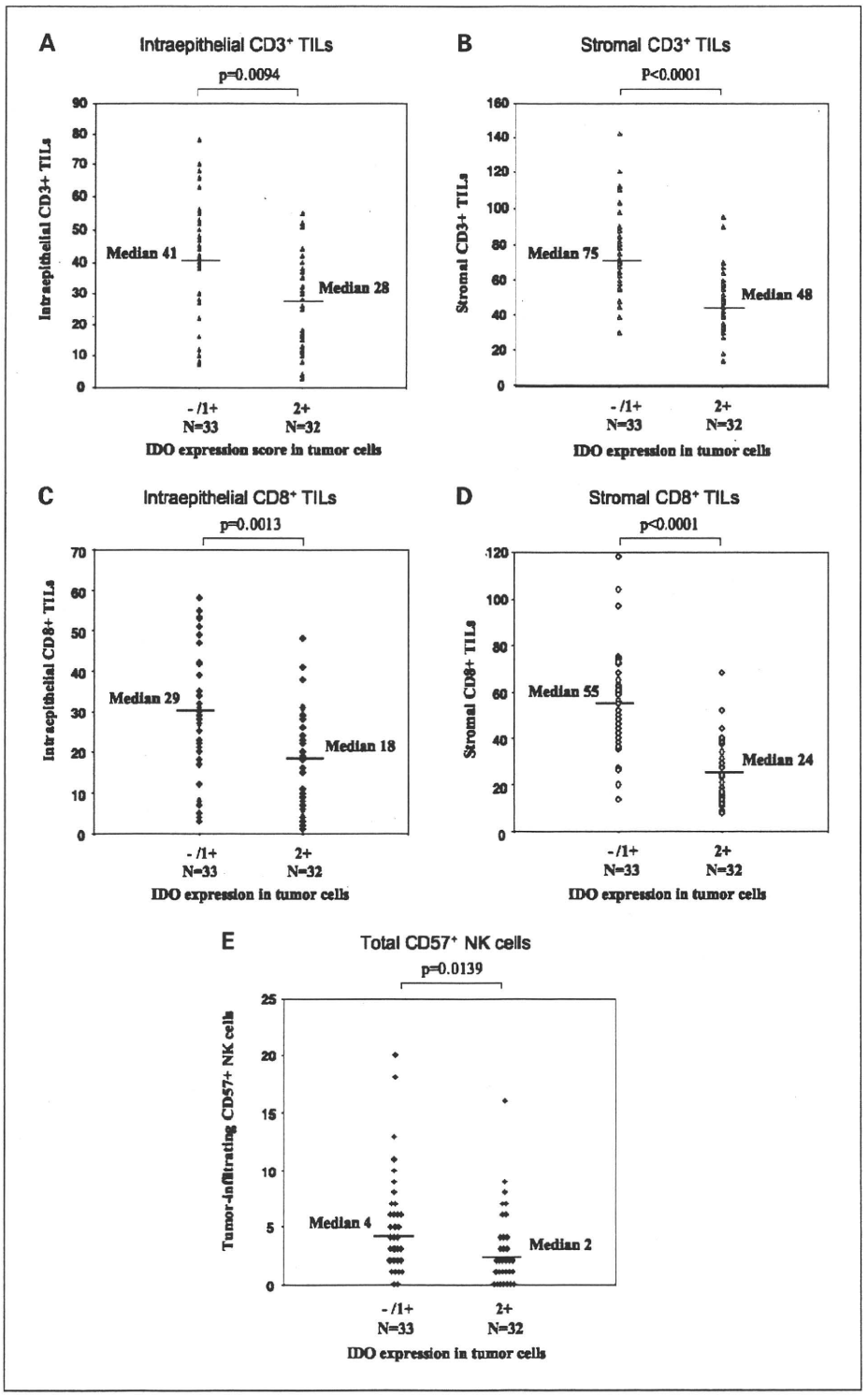

Fig. 2. Association of IDO expression with the number of TIL and NK cells. *A*, intraepithelial CD3+ TILs; *B*, stromal CD3+ TILs; *C*, intraepithelial CD8+ TILs; *D*, stromal CD8+ TILs; *E*, total CD57+ NK cells. There was a significant difference in the number of TIL and NK cells between the IDO-/IDO1+ tumors and IDO2+ tumors.

DOI:10.1158/1078-0432.CCR-07-4144

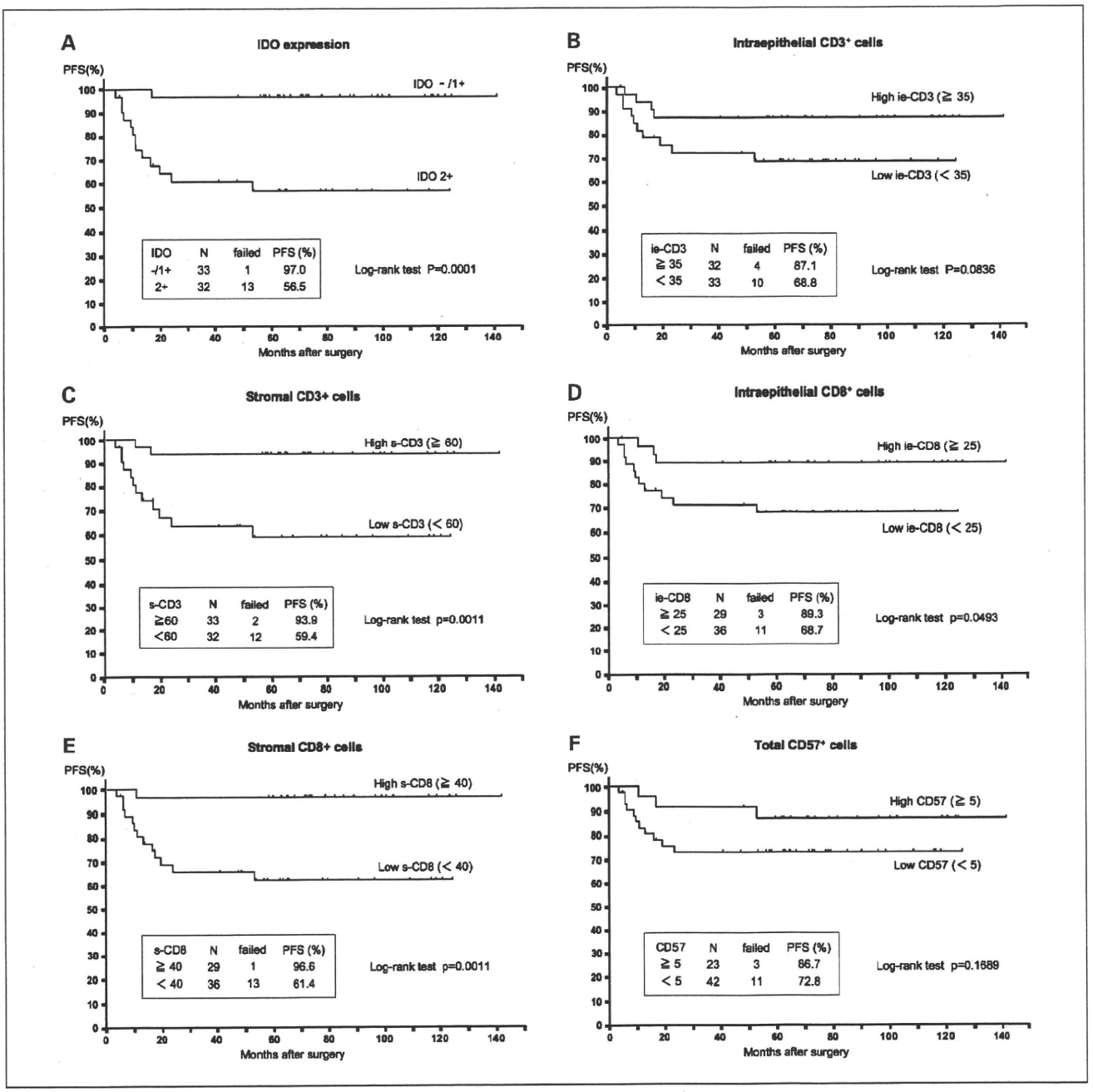

Fig. 3. PFS curves in endometrial cancer patients according to IDO expression (*A*), intraepithelial CD3+ cell count (*B*), stromal CD3+ cell count (*C*), intraepithelial CD8+ cell count (*D*), stromal CD8+ cell count (*E*), and total CD57+ NK-cell count (*F*). Significant differences in the PFS were found for IDO expression ($P = 0.0001$), stromal CD3 ($P = 0.0011$), intraepithelial CD8 ($P = 0.0493$), and stromal CD8 ($P = 0.0011$).

tumor-infiltrating T cells and NK cells using serial tissue sections from 65 patients, and also analyzed the prognostic effect of both IDO and the TIL count.

There have been many reports indicating that the presence of CD3+ or CD8+ TILs correlates with favorable clinical outcome (22–25). In addition to TILs, recent studies have shown that the presence of tumor-infiltrating CD57+ NK cells also correlates with better prognosis in patients with various cancers (17–20). These studies suggest that both cytotoxic T cells and NK cells may play an important role in immune surveillance in cancer patients and have significant antitumor activity. In the present study, we analyzed the infiltration of TILs by separating them into two groups (intraepithelial and stromal) and then evaluating the relationship between tumoral IDO expression and TIL counts in each area. Interestingly, tumors with high IDO expression had significantly reduced numbers of both intraepithelial and stromal CD3+ or CD8+ cells. This is consistent with a recent report showing the association of IDO expression with a reduction of CD3+ lymphocytes in colorectal cancer (14). Furthermore, our data showed that tumors with high IDO expression had a significantly reduced number of CD57+ cells. These findings suggest that tumoral

DOI:10.1158/1078-0432.CCR-07-4144

IDO expression is associated with the suppressed infiltration of both cytotoxic T cells and NK cells into the tumor epithelium and adjacent stroma, which may contribute to the progression of endometrial cancer.

Recently, two possible mechanisms for the immunosuppressive action of IDO in tumor-bearing hosts have been proposed (2); it is thought that IDO expressed by tumor cells can create a localized immunosuppressive status within the tumor microenvironment (effector phase) either by suppressing proliferation and function of TILs via tryptophan depletion or by directly killing them using toxic catabolites of tryptophan, such as kynurenine. Alternatively, host antigen-presenting cells expressing IDO may pick up tumor-derived antigens and migrate into tumor-draining lymph nodes (priming phase) where they cannot effectively prime naive T cells, resulting in the failure of clonal expansion of effector T cells. Our present study showed that IDO was dominantly localized to tumor cells in endometrial cancer tissues, suggesting that tumor-derived IDO rather than IDO-positive antigen-presenting cells may primarily regulate local immune function at the effector phase, where IDO might induce the surrounding effector T cells or NK cells into apoptosis and delete them by creating a tryptophan-depleted, tryptophan catabolite–rich environment (5, 26). This hypothesis may be supported by Uyttenhove et al. (7) showing that IDO-expressing tumors induce a lack of specific T-cell accumulation at the tumor site in mice and can block T-cell proliferation locally. However, further studies are needed to clarify the mechanism for the involvement of tumoral IDO in suppression of TILs in human cancer.

The present study showed that patients with high IDO expression, as well as low numbers of stromal CD3+, intraepithelial CD8+, and stromal CD8+ TILs, had significantly impaired PFS. These data are consistent with a previous report showing the prognostic significance of CD8+ TILs in endometrial carcinoma (24). Furthermore, our multivariate analyses showed that both IDO expression and the number of stromal CD3+ TILs were independent prognostic factors for impaired PFS. These findings indicate that patients having tumors with high IDO expression and less TIL infiltration are more likely to experience recurrence and have poor prognosis. Because over 70% of endometrial cancer patients present the early-stage of the disease and most of them are curable with surgery alone (27), it would be of substantial benefit to define the minority of patients who are likely to experience recurrence and also to give adjuvant therapy to these patients alone. Our data suggest that the expression level of IDO in combination with the TIL count

Table 2. Univariate and multivariate analyses of overall survival and PFS

Variable	Overall survival			PFS		
	Univariate	Multivariate		Univariate	Multivariate	
	P	HR (95% confidence interval)	*P*	*P*	HR (95% confidence interval)	*P*
Age						
<60		(—)			(—)	
≥60	0.151	(—)		0.088	(—)	
FIGO stage						
I/II		1			1	
III/IV	0.002	2.456 (1.423-14.266)	0.032	0.001	3.878 (1.252-12.011)	0.019
Grade						
G1-G2		(—)			(—)	
G3	0.132	(—)		0.490	(—)	
Myometrial invasion						
≤50%		(—)			(—)	
>50%	0.070	(—)		0.114	(—)	
Nodal status						
Negative		1			1	
Positive	0.001	4.904 (1.210-19.877)	0.026	0.010	1.185 (0.218-4.831)	0.712
LVSI						
Absent		1			1	
Present	0.020	2.919 (0.495-17.204)	0.237	0.031	1.268 (0.309-5.200)	0.742
IDO expression						
None/Low		1			1	
High	0.024	6.650 (0.738-59.931)	0.091	0.005	6.317 (1.728-54.800)	0.025
Intraepithelial CD3+						
≥35		(—)			(—)	
<35	0.089	(—)		0.096	(—)	
Stromal CD3+						
≥60		(—)			1	
<60	0.055	(—)		0.006	3.693 (1.790-17.277)	0.047
Intraepithelial CD8+						
≥25		(—)			(—)	
<25	0.146	(—)		0.044	2.255 (0.459-18.078)	0.238
Stromal CD8+						
≥40		1			1	
<40	0.041	3.594 (0.314-41.140)	0.304	0.012	1.710 (0.110-26.579)	0.902
Total CD57+						
≥5		(—)			(—)	
<5	0.116	(—)		0.182	(—)	

DOI:10.1158/1078-0432.CCR-07-4144

not only reflects the local immunologic status within tumors, but also can become a reliable prognostic indicator for endometrial cancer. Moreover, it may contribute to the individualization of adjuvant therapy.

Immune escape is a crucial feature of cancer progression, and recent work has identified several important molecules/factors that are involved in tumor-induced immunosuppressive mechanisms, including IDO, programmed cell death 1 ligand 1 (28), and CD4+CD25+FOXP3+ regulatory T cells (29). Furthermore, a close relationship between IDO expression and the occurrence of regulatory T cells in tumors was shown (30, 31). Thus, much attention has been paid to overcoming the immune tolerance created by these factors as a novel strategy for cancer therapy (32). The evidence shown in this paper that high IDO expression is associated with a reduced TIL count and also with a poor clinical outcome could make IDO an attractive new target for the treatment of endometrial cancer. Recent studies in mice showed that combinations of IDO inhibitors with chemotherapeutic agents or irradiation synergistically enhanced antitumor activity by reversing the suppression of T cells, suggesting that IDO inhibitors might have utility as anticancer agents (10, 11). Future preclinical and clinical studies are needed for therapeutic application of IDO inhibitors in human cancer.

In conclusion, we showed here that tumoral IDO expression correlated with suppressed infiltration of T cells and NK cells in endometrial cancer tissues, which is associated with disease progression and impaired clinical outcome. Although the precise function of tumoral IDO in human cancer remains to be elucidated, our findings suggest that targeting IDO to restore host antitumor immunity may be a novel therapeutic strategy for endometrial cancer.

References

1. Whiteside TL. Immune suppression in cancer: effects on immune cells, mechanisms and future therapeutic intervention. Semin Cancer Biol 2006;16:3–15.
2. Munn DH, Mellor AL. Indoleamine 2,3-dioxygenase and tumor-induced tolerance. J Clin Invest 2007;117:1147–54.
3. Takikawa O. Biochemical and medical aspects of the indoleamine 2,3-dioxygenase-initiated L-tryptophan metabolism. Biochem Biophys Res Commun 2005;338:12–9.
4. Munn DH, Zhou M, Attwood JT, et al. (1998) Prevention of allogeneic fetal rejection by tryptophan catabolism. Science 1998;281:1191–93.
5. Frumento G, Rotondo R, Tonetti M, Damonte G, Benatti U, Ferrara GB. Tryptophan-derived catabolites are responsible for inhibition of T and natural killer cell proliferation induced by indoleamine 2,3-dioxygenase. J Exp Med 2002;196:459–68.
6. Della Chiesa M, Carlomagno S, Frumento G, et al. The tryptophan catabolite L-kynurenine inhibits the surface expression of NKp46- and NKG2D-activating receptors and regulates NK-cell function. Blood 2006;108:4118–25.
7. Uyttenhove C, Pilotte L, Theate I, et al. Evidence for a tumoral immune resistance mechanism based on tryptophan degradation by indoleamine 2,3-dioxygenase. Nat Med 2003;9:1269–74.
8. Mellor AL, Munn DH. IDO expression by dendritic cells: tolerance and tryptophan catabolism. Nat Rev Immunol 2004;4:762–74.
9. Munn DH, Sharma MD, Hou D, et al. Expression of indoleamine 2,3-dioxygenase by plasmacytoid dendritic cells in tumor-draining lymph nodes. J Clin Invest 2004;114:280–90.
10. Muller AJ, DuHadaway JB, Donover PS, Sutanto-Ward E, Prendergast GC. Inhibition of indoleamine 2,3-dioxygenase, an immunoregulatory target of the cancer suppression gene Bin1, potentiates cancer chemotherapy. Nat Med 2005;11:312–9.
11. Hou DY, Muller AJ, Sharma MD, et al. Inhibition of indoleamine 2,3-dioxygenase in dendritic cells by stereoisomers of 1-methyl-tryptophan correlates with antitumor responses. Cancer Res 2007;67:792–801.
12. Okamoto A, Nikaido T, Ochiai K, et al. Indoleamine 2,3-dioxygenase serves as a marker of poor prognosis in gene expression profiles of serous ovarian cancer cells. Clin Cancer Res 2005;11:6030–9.
13. Astigiano S, Morandi B, Costa R, et al. Eosinophil granulocytes account for indoleamine 2,3-dioxygenase-mediated immune escape in human non-small cell lung cancer. Neoplasia 2005;7:390–6.
14. Brandacher G, Perathoner A, Ladurner R, et al. Prognostic value of indoleamine 2,3-dioxygenase expression in colorectal cancer: effect on tumor-infiltrating T cells. Clin Cancer Res 2006;12:1144–51.
15. Ino K, Yoshida N, Kajiyama H, et al. Indoleamine 2,3-dioxygenase is a novel prognostic indicator for endometrial cancer. Br J Cancer 2006;95:1555–61.
16. Takikawa O, Kuroiwa T, Yamazaki F, Kido R. Mechanism of interferon-γ action. Characterization of indoleamine 2,3-dioxygenase in cultured human cells induced by interferon-γ and evaluation of the enzyme-mediated tryptophan degradation in its anticellular activity. J Biol Chem 1988;263:2041–8.
17. Coca S, Perez-Piqueras J, Martinez D, et al. The prognostic significance of intratumoral natural killer cells in patients with colorectal carcinoma. Cancer 1997;79:2320–8.
18. Ishigami S, Natsugoe S, Tokuda K, et al. Prognostic value of intratumoral natural killer cells in gastric carcinoma. Cancer 2000;88:577–83.
19. Villegas FR, Coca S, Villarrubia VG, et al. Prognostic significance of tumor infiltrating natural killer cells subset CD57 in patients with squamous cell lung cancer. Lung Cancer 2002;35:23–8.
20. Menon AG, Janssen-van Rhijn CM, Morreau H, et al. Immune system and prognosis in colorectal cancer: a detailed immunohistochemical analysis. Lab Invest 2004;84:493–501.
21. Sedlmayr P, Blaschitz A, Wintersteiger R, et al. Localization of indoleamine 2,3-dioxygenase in human female reproductive organs and the placenta. Mol Hum Reprod 2002;8:385–91.
22. Naito Y, Saito K, Shiiba K, et al. CD8+ T cells infiltrated within cancer cell nests as a prognostic factor in human colorectal cancer. Cancer Res 1998;58:3491–4.
23. Zhang L, Conejo-Garcia JR, Katsaros D, et al. Intratumoral T cells, recurrence, and survival in epithelial ovarian cancer. N Engl J Med 2003;348:203–13.
24. Kondratiev S, Sabo E, Yakirevich E, Lavie O, Resnick MB. Intratumoral CD8+ T lymphocytes as a prognostic factor of survival in endometrial carcinoma. Clin Cancer Res 2004;10:4450–6.
25. Sato E, Olson SH, Ahn J, et al. Intraepithelial CD8+ tumor-infiltrating lymphocytes and a high CD8+/regulatory T cell ratio are associated with favorable prognosis in ovarian cancer. Proc Natl Acad Sci U S A 2005;102:18538–43.
26. Fallarino F, Grohmann U, Vacca C, et al. T cell apoptosis by tryptophan catabolism. Cell Death Differ 2002;9:1069–77.
27. Creutzberg CL, van Putten WL, Koper PC, et al. Surgery and postoperative radiotherapy versus surgery alone for patients with stage-1 endometrial carcinoma: multicentre randomised trial. Lancet 2000;355:1404–11.
28. Hamanishi J, Mandai M, Iwasaki M, et al. Programmed cell death 1 ligand 1 and tumor-infiltrating CD8+ T lymphocytes are prognostic factors of human ovarian cancer. Proc Natl Acad Sci U S A 2007;104:3360–5.
29. Curiel TJ, Coukos G, Zou L, et al. Specific recruitment of regulatory T cells in ovarian carcinoma fosters immune privilege and predicts reduced survival. Nat Med 2004;10:942–9.
30. Nakamura T, Shima T, Saeki A, et al. Expression of indoleamine 2, 3-dioxygenase and the recruitment of Foxp3-expressing regulatory T cells in the development and progression of uterine cervical cancer. Cancer Sci 2007;98:874–81.
31. Sharma MD, Baban B, Chandler P, et al. Plasmacytoid dendritic cells from mouse tumor-draining lymph nodes directly activate mature Tregs via indoleamine 2,3-dioxygenase. J Clin Invest 2007;117:2570–82.
32. Gajewski TF. Identifying and overcoming immune resistance mechanisms in the melanoma tumor microenvironment. Clin Cancer Res 2006;12:2326s–30s.